The Sailing Tug

A feasibility study on the application of Wind-Assisted towing of the Thialf

B.A.M. Vos

01-07-2019

TU Delft

MARINE CONTRACTORS

The Sailing Tug

A feasibility study on the application of Wind-Assisted towing of the Thialf

by

B.A.M. Vos

to obtain the degree of Master of Science
at the Delft University of Technology,
Faculty of Mechanical, Maritime and Materials Engineering
to be defended publicly on Wednesday July 10, 2019

Student number: 4012542
Project duration: October 1, 2017 – July 10, 2019
Thesis committee:

Prof. ir. J.J. Hopman,	TU Delft
Dr. ir. I. Akkerman,	TU Delft
Dr. ir. A. Vrijdag,	TU Delft
Ir. P. Meeuws,	HMC

MARINE CONTRACTORS

TU Delft

Abstract

The international maritime sector accounts for about 2% of all global carbon dioxide (CO2) emissions, the main greenhouse gas that causes global warming. Nations meeting at the United Nations International Maritime Organization (IMO) in London have proposed an initial strategy for the reduction of greenhouse gas (GHG) emissions from ships, setting out to reduce GHG emissions from international shipping by phasing them out as soon as possible with the aim to achieve zero emission by the end of this century[1]. Heerema Marine Contractors (HMC) is a world leading marine contractor in the international offshore energy industry and aims to be a role model in environmental responsibility through carbon emission reductions[2].

As a result of HMC's global activities, their fleet covers a considerable distance through transit across the globe. Their large semi-submersible crane vessels are conventionally transported through towing by a tug. The great amounts of fuel required for these transits provides a significant opportunity for the reduction of HMC's carbon footprint. One such initiative proposed within HMC is the application of wind-assisted ship propulsion on the tow configuration.

This report presents an initial investigation of the feasibility of wind-assisted towing of the HMC's Thialf, a semi-submersible crane vessel. Previous internal research at HMC showed the feasibility of using a discarded Panamax vessel as a floating breakwater. While operationally the discarded Panamax was found to be feasible, economically this was not the case. In this research, using the Panamax as a wind-assisted tug for towing the Thialf is investigated. As such the Panamax vessel can be employed for multiple purposes; for wind-assisted towing and as a floating breakwater, improving the financial feasibility.

To test the performance of a wind-assisted tow operation, a comprehensive 2D model is developed in this research to be able to check configuration variations in a wind-assisted tow setup. A conceptual design of a Panamax vessel converted into a sailing tug is implemented in a 2D model simulation. The performance in combination with the Thialf is assessed under the common environmental conditions experienced by the Thialf for various transit routes.

Results showed that the use of a wind-assisted tow configuration based on a Panamax, without using the Thialf propulsion is not feasible. The main point of failure is the required force balance transverse to the sailing direction.The Panamax basis used for the preliminary wind-assisted tug design proved to be not the optimal base case due to the limited leeward force generation under a drift angle and the large sensitivity to environmental loading. Although implemented measures improved the systems performance, it is debatable whether a wind-assisted tow configuration with the associated uncertainties is the most promising area to accomplish significant CO2 reductions.

[1] http://www.imo.org/en/MediaCentre/PressBriefings/Pages/06GHGinitialstrategy.aspx
[2] https://hmc.heerema.com/about/sustainability/

List of symbols

Symbol	Description
α_c	Current angle of attack
α_w	Wind angle of attack
α_{wave}	Wave angle of attack
α_r	Effective rudder inflow angle
β	drift angle
γ	Apparent direction
δ	Rudder angle relative to the ship centerline
ϵ	Sail trim angle
θ	Towline angle
ω_e	encounter frequency
ω	wave frequency
ξ	Coverage
ρ	density
∇	Displacement
ϕ	Heeling angle
Λ	Rudder aspect ratio
g	Acceleration due to gravity
n	Propeller RPM
A	area
AR	Effective aspect ratio $(2S^2/A)$
$\overline{BN_\phi}$	Buoyency - Metacentre
$\overline{BM}$	Buoyency - Initial Metacentre
C_b	Hull block coefficient
C_n	Rudder normal force coefficient
$C_{T,c,x}$	Thialf x current coefficient
$C_{T,c,y}$	Thialf y current coefficient
$C_{T,c,z}$	Thialf z current coefficient
$C_{T,w,x}$	Thialf x wind coefficient
$C_{T,w,y}$	Thialf y wind coefficient
$C_{T,w,z}$	Thialf z wind coefficient
$C_{T,wave,x}$	Thialf x wave coefficient
$C_{T,wave,y}$	Thialf y wave coefficient
$C_{T,wave,z}$	Thialf z wave coefficient
D_p	Propeller diameter

Table 1: Symbols

F_n	rudder normal force
$F_{T,X}$	Global X-Force working on Thailf
$F_{T,Y}$	Global Y-Force working on Thailf
$F_{P,X}$	Global X-Force working on Panamax
$F_{P,Y}$	Global Y-Force working on Panamax
$F_{T,c,x}$	Thialf force by current in x-direction
$F_{T,c,y}$	Thialf force by current in y-direction
$F_{T,w,x}$	Thialf force by wind in x-direction
$F_{T,w,y}$	Thialf force by wind in y-direction
$F_{T,wave,x}$	Thialf drift force by waves in x-direction
$F_{T,wave,y}$	Thialf drift force by waves in y-direction
$\overline{GM}$	Initial Metacentre Height
$\overline{GZ}$	rightening arm
$\overline{GN_\phi}$	Centre of gravity - Metacentre
H_s	Significant wave height
I_t	Transverse waterplane area of Inertia
J	Advance ratio
$\overline{KB}$	Keel - Centre of Buoyency
$\overline{KG}$	Keel - Centre of Gravity
K_t	Propeller thrust coefficient
M_r	Restoring Moment
M_e	External Moment
$M_{T,c,z}$	Thialf moment by current around vessel z-axis
$M_{T,w,z}$	Thialf moment by wind around vessel z-axis
$M_{T,wave,z}$	Thialf moment by waves around vessel z-axis
T	Propeller Thrust
T_e	Encounter period
U_r	induced velocity at rudder
V_a	Apparent velocity
V_{true}	Global velocity
V_i	Inflow velocity
W_p	Wake fraction at propeller

Table 2: Symbols

Abbreviations

Abbreviation	Description
HMC	Heerema Marine Contractors
WASP	Wind Assisted Ship Propulsion
OPEX	Operation Expenditure
CAPEX	Capital Expenditure
MCS	Moving Coordinate System
VCS	Vessel Coordinate System
TCS	Thialf Coordinate System
PCS	wind assisted Panamax Coordinate System
SSCV	Semi Submersible Crane Vessel
VVP	Velocity Prediction Program
DWT	Dead Weight Tonne
IMO	International Marine Organization
CPP	Controllable Pitch Propeller
FPP	Fixed Pitch Propeller
IMO	International Marine Organisation
DPR	Daily Progress Report
MW	MegaWatt
RPM	Rounds Per Minute
GM	Metacentre Height
KB	Keel Buoyence distance
BM	Buoyency Metacentre
OCIMF	Oil Companies International Marine Forum
MCR	Maximum Continuous Rating
IMCA	International Marine Contractors Association
AoA	Angle of Attack
BAR	Blade Area Ratio
MCA	Multi Criteria Analyses
RANSE	Reynolds-Averaged Navier-Stokes Equations

Table 3: Abbreviations

Coordinate and Direction Conventions

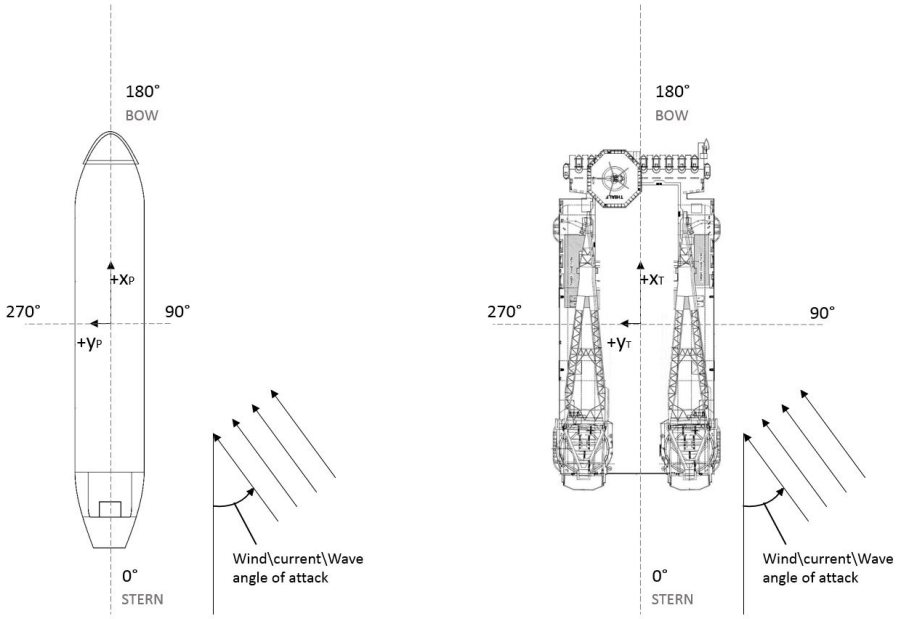

Figure 1: Vessel-specific coordinate and direction convention

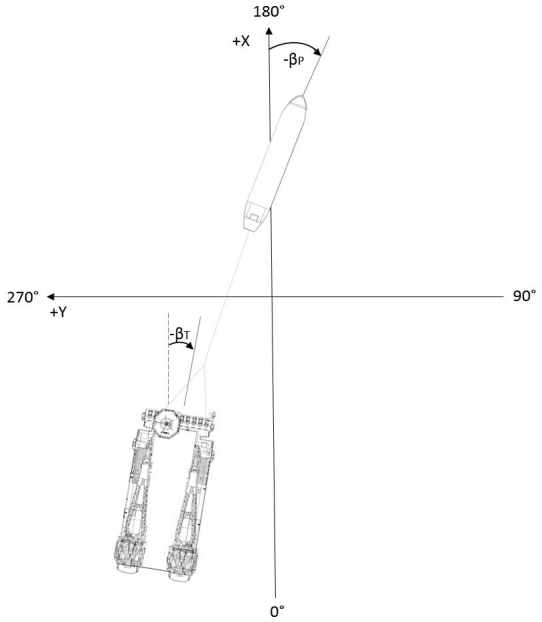

Figure 2: Moving frame coordinate and direction convention

Contents

1

Introduction

Recently, a renewed interest in wind-assisted Ship Propulsion (WASP) has emerged. In the past, during the early days of international shipping wind propulsion was the proven way. However, with the invention of the steam and diesel engines these forms of ship propulsion took over throughout the 20th century. It was the 1980's oil crisis that brought back the attention to WASP however, this did not yet lead to a major uptake of wind propulsion. In recent years, the increased environmental concerns and associated pressure to reduce carbon emissions have been the key drivers for a renewed interest in WASP.

So far, various initiatives in WASP have been implemented for new-built vessels as well as conversions of existing vessels i.e. retrofits. Examples of new-built initiatives include the WASP Ecoliner (Architects, 2013) the E-Ship 1 (Traut et al., 2014) and the Estraden (Kuuskoski, 2017). Previous retrofits include the Viking Grace, the Fehn Pollux and the Maersk Tanker. However, empirical studies on WASP are lacking such that the application of WASP needs further investigation.

This graduation research is commissioned by Heerema Marine Contractors (HMC), an offshore heavy lift contractor that offers a wide range of services from construction, transportation, installation to decommissioning of offshore structures. Their fleet includes Semi-Submersible Crane Vessels (SSCV's) active around the globe. With the development of WASP possibilities and increased environmental concerns, HMC is interested in the potential application of WASP. Therefore, this research focuses on investigating the feasibility of applying WASP to HMC's fleet.

In this chapter, the motivation for this research is further elaborated on, followed by a description of the research question and project approach. Finally, an outline of the report structure is provided.

1.1. Research Motivation

Heerema Marine Contractors provides extreme heavy lift services all over the world. For these world-wide services, HMC employs their semi-submersible crane vessels: the Thialf, Balder, Hermod and the soon to be finished Sleipnir. As a result of their global activity, these SSCV's are a considerable time in transit. Such transit requires a great amount of fuel and provides a significant opportunity for the reduction of HMC's operating carbon footprint. For example, for the Thialf the propulsion for transit is currently delivered through six thrusters present under the hull and one 200-tonne bollard-pull tug vessel. Together, it is estimated that these require 175 m^3 MDO per day in transit.

To investigate reduction of the carbon footprint of the transit of HMC's SSCV's, this research will examine the application of WASP for the transit of the Thialf specifically. For transit of

the Thialf, the application of WASP can be investigated for the direct propulsion from the Thialf or the propulsion for the vessel operated to tow the Thialf. Replacing direct propulsion of the Thialf with WASP requires the placement of large sails. However, as the deckspace of the Thialf is required for operation activities and the placement of large sails could disrupt free movement of the cranes, the opportunities for replacing direct propulsion of the Thialf with WASP are limited. Therefore, this research focuses on the application of WASP for the tug vessel i.e. wind-assisted Towing. Due to their small size, the pull tug vessels currently employed for towing the Thialf are unsuitable for WASP-operated transit. Therefore, an alternative tow setup needs to be investigated for WASP-operated towing of the Thialf.

With the new Panama canal becoming available, it is expected that the existing Panamax vessels will become available at attractive costs. Therefore, previous graduation research has investigated a discarded Panamax vessel as a basis for a floating breakwater solution for HMC (Smulders, 2017). The large size and stability of the Panamax vessels makes them potentially well-suited for WASP. Therefore, this research carries forward upon the research from Smulders (2017), by investigating the use of a discarded Panamax vessel for HMC as a basis for WASP transit of the Thialf. More specifically, this research investigates the feasibility of equipping a discarded Panamax bulk carrier with WASP to decrease cost and emissions during voyages, and accordingly using it as a tug during the transit of the Thialf.

1.2. Research Question

The goal of this research is to study the feasibility of replacing the conventional tow configuration of the Thialf with a wind-assisted Tow configuration. Specifically, the aim is to investigate the feasibility of using a wind-assisted Panamax vessel for towing the Thialf. To do so, a preliminary conversion design for a wind-assisted Panamax vessel, further referred to as the Sailing Tug, will be presented. Subsequently, the performance of the Sailing Tug - Thialf configuration will be assessed under operating conditions based on transit speed. Therefore, we aim to answer the following research question:

Is it feasible to replace the Tug present in a conventional tow configuration by a wind-assisted Tow Vessel and tow the Thialf without using its own installed thrusters?

Where we define a feasible towing configuration as a configuration that achieves a velocity above zero, for relative wind direction $\alpha_w < 135^\circ$ $\alpha_w > 225^\circ$, presenting a 90°allowable no-go area in for head wind. This will allow the system to reach any destination when tacking is taken into account. To answer the research question, a Velocity Prediction Program (VPP) will be designed that translates the input of environmental conditions into the maximum achievable transit sailing speed of the Thialf in a chosen direction. As part of this VPP, 2D simulations of the Sailing Tug-Thialf combination will be used to determine the required force and moment balances. For an overview of the system performance under every wind angle, the outcomes of the VPP are visualized through polar diagrams.

1.3. Report Outline

The report starts with an examination of the current characteristics of the conventional HMC tow configuration and the available wind conversion systems on the market in Chapter 2. The findings are used to propose a design of a wind-assisted tow operation.

Chapter 3 will elaborate on the forces and moments present in a wind-assisted tow operation and how these can be approximated for the use in a 2D tow operation simulation. With the input gathered in chapter 3, a balance solving strategy with a corresponding computer model is proposed. The governing equations are introduced in Chapter 4, and an overview of the model is presented in the form of a block diagram.

A method to verify the intermediate results and output of the model together with the verification results are presented in Chapter 5.

After the verification the results from the complete system are presented in Chapter 6 which will be used to answer the research question. Based on the outcome of the model, multiple system improvements are tested to get an overview of possible areas of improvement.

In Chapter 7 the results are discussed and a conclusion on the feasibility of wind-assisted towing within HMC is drawn.

2

Literature Review and Tug Design

This research investigates the feasibility of the Sailing Tug-Thialf configuration, a wind-assisted tow operation. To be able to propose such a new form of towing, a good understanding of the conventional Thialf transit operation is necessary. Therefore, this chapter begins with a review of the conventional ocean transit in section 2.1. Subsequently, alternative wind-assisted propulsion solutions are investigated and compared in section 2.2. As the main source of propulsion for the Sailing Tug will be the wind conversion system on deck, the section focuses on possible alternatives for on-deck wind conversion. The most promising alternative is chosen and will be employed for the preliminary design of the Sailing Tug throughout the remainder of this research. Finally, in section 2.3 the design of the Sailing Tug, a converted wind-assisted Panamax vessel, will be proposed and elaborated on.

2.1. Conventional Ocean Transit

The conventional ocean transit procedure consists of the Thialf being towed by one of HMC's tug vessels: the Kolga or Bylgia. The Thialf and tug are connected by a towline-bridle combination as illustrated in figure 2.1. The length of the bridle leg is fixed at 41 meters, and the length of the main towline is varied dependent on operational conditions, mostly around 800m - 1000m. In the conventional towing configuration, the two controllable pitch propellers of the tug and the six retractable thrusters of the Thialf are used for propulsion.

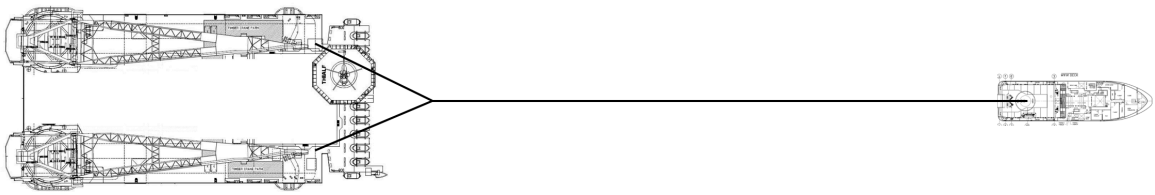

Figure 2.1: Overview of the Thialf-Kolga tow combination

To determine the average transit speed and the fuel consumption of the conventional transit procedure of the Thialf, the propulsion properties of the Kolga and Thialf as presented in Table 2.1 are examined.

Name	Kolga	Thialf
Type	Kaplan KC	Wageningen ka 5-75
Nozzle	19A	19A
number of blades	4	5
BAR	0.55	0.75
Diameter	4.1	3.4
Pitch type	CPP	FPP
RPM	150	199
Installed Power (kW)	12000	33000
Bollard Pull (tonne)	200	400
avg. transit Consumption (m3/day)	50	125

Table 2.1: Propulsion properties of the Kolga and Thialf derived from internal HMC sources

With the specifications from Table 2.1, internal HMC sources indicate that the Kolga is able to provide a 200 tonne bollard pull. From Daily Progress Reports (DPR) it is derived that per 24 hours of towing, the Kolga consumes approximately $50m^3$ and the Thialf 125 m^3 of MDO. Internal HMC sources indicate that the Hotel load of the Thialf is 2,25 MW, for which one out of 12 diesel generators is needed. Moreover, the Hotel fuel consumption is 10 m^3 per day. Finally, the average transit speed over the 2017 voyages for the Thialf is found to be six knots.

2.2. Wind Propulsion

Wind propulsion for ships has been a widely proven concept as of thousands of years. Today, a wide variety of wind propulsion systems are available which have seen improvements over the years and new concepts are still being developed. The wind conversion systems can be divided into three categories: Soft sails, Wing sails and Active sails.

2.2.1. Soft Sails

Soft sails are the oldest and most common type of wind propulsion since their invention and most probably will remain the standard for leisure crafts for the coming decades. Over the enormous time-span during which these sails have been used, extensive knowledge has been gained about their behavior and performance. As the name suggests, the Soft sails are composed of flexible material, making it more sensitive to wear and tear. Within the soft sails come in different sizes and shapes, the 5 most common types are assessed: the Square rig, Bermuda rig, Dyna rig, Aero rig and Kite.

- The Square rig yields a maximum lift coefficient of 1.6 with a drag coefficient of 1 for a 90°angle of attack (Bergeson and Greenwald, 1985). The Square rig dates back to more than 2,000 years ago and their wide availability and relative simplicity makes them low in cost, but operation requires a large crew and maintenance costs is high. Furthermore, the system operates at limited wind conditions since the upwind performance is poor. The system can be easily scaled up due to the limited mass of additional sail area.
- The Bermuda rig is found on the majority of sailing yachts but tends to have poor lift distribution due to the triangular shape of the sails. The maximum lift capacity is 1.5 with an associated drag coefficient of 0.91 (Bergeson and Greenwald, 1985). The simple construction results in a low cost to built. Although less crew is required to control the fewer separate sails compared to a Square rig, a relatively large crew is still necessary.
- The Dyna rig has a high aerodynamic performance for a soft sail with a maximum lift coefficient of 1.8 at a drag coefficient of 0.85, requires little maintenance, has a high safety and ease of use as it can be controlled single-handedly from the bridge (Dykstra, 2017). To avoid any obstruction of the sail area a very stiff mast is required increasing the cost of this system.
- The Aero rig has the highest performance when compared to a three-mast schooner, Dyna rig and Bermuda rig (Nijsten and Vos, 2002), and improves the sail surface per-

pendicular to the wind by the attachment of the jib to the horizontal boom. The maximum lift coefficient is 1.9 at an associated drag coefficient of 0.75. The single rotating mast being the only connection to the vessel makes it a system that is relatively easy to control but this increases the cost of the system as this rotation point needs to be able to transfer all forces and moments from the sail to the vessel.

- The Kite has limited sailing angles compared to other sails and was found not to be feasible on HMC SSCV's due to relatively low thrust contribution of the towing Kite, large required investment and replacement costs and low durability of the Kite (Troll, 2010). Due to the drop in oil price since 2010, it is assumed that the towing Kite is still not a feasible solution for the application on SSCV's.

2.2.2. Wingsails

Since 2013, Wingsails have been the choice for the Americas cup. With the solid two-piece wings the boats are capable of sailing twice as fast as the wind. Wingsails have many similarities with the wings of an airplane, but the most important difference is that a wing sail needs to be able to provide lift on both sides of the sail. The maximum lift coefficient for Wingsails is found to be 2.1 with an associated drag coefficient of 0.7 (Nijsten and Vos, 2002). Wingsails have few moving parts such that they are able to withstand harsh weather conditions, and the hard material make them durable. Wingsails can be operated from a distance as only the vertical orientation is controlled. The absence of reef capabilities decreases the maximum survival wind velocity.

2.2.3. Active Sails

For this research, two categories of active sail types are examined: the Flettner rotors and Turbosails. A Flettner rotor is a smooth cylinder with disc end plates which is spun along its long axis and, as air passes at right angles across it, the Magnus effect causes an aerodynamic force perpendicular to the direction of attack (Brockett, 1964). In a rotor ship the rotors are placed vertically and lift is generated at right angles to the wind, to drive the ship forwards. The only parameter which can be controlled is the rotation speed, making it easy to control but there is no method to influence the exact direction of the force. The bearings at the bottom of the The large rotating cylinders are relatively sensitive to wear as the gyroscopic effect of the cylinders creates a moment on them when the vessel is rolling and pitching at sea. Traut et al. (2014) indicate a maximum lift coefficient of 7.5. at a drag coefficient of 2.2. There are a few examples of rotor ships in operation at the moment.

The highest lift to drag ratio was created with a mechanical sail using aspiration power, known as a Turbosail, introduced by J.A. Cousteau (1985). This foil can generate about 3 times higher lift compared to conventional foils, which do not use active suction of the boundary layer. The main advantage over a regular solid wing design is the relative increase in lift compared to the drag force. Under most angels of attack of the wind, the lift causes the propulsive force where the drag coefficient causes the heeling moment. The ventilator which provides the suction force for this system is placed inside the solid structure protected from external conditions. The Turbosail orientation and suction power can both be controlled from the bridge of a vessel. J.A. cousteau built two vessels based on the concept of a Turbosail.

2.2.4. Comparison of Wind Conversion Systems

To decide which system is most promising for the application on the Sailing Tug, the systems are compared through a Multi-Criteria Analysis. Based on internal consultation with HMC sources, the following eight criteria were selected in comparing the wind conversion systems:

1. Propulsive performance
   Since the goal is to develop a configuration that is capable to sail every direction relative to the wind, the propulsive performance is most important at this stage of the research. When a configuration proves to have sufficient performance, the wind conversion system in the simulation can easily be changed to a system with a higher score on other criteria.

The lift coefficient provides the force component perpendicular to the wind direction, the drag coefficient for the component in line with the wind. For most sail angles, the lift component yields a force component partly in the sailing direction while the drag component provides an undesirable force in the opposite direction. Therefore, the propulsive performance is defined as the lift coefficient divided by the drag coefficient at the angle that yields the maximum lift. Since the goal is to develop a configuration that is capable to sail in every direction relative to the wind, the propulsive performance is most important criteria for selecting the wind conversion system and will be provided the highest weight factor.

2. Robustness
   High robustness of the system is required, as the system needs to be able to withstand the harsh conditions at sea. To aboard a transit mission because of failure of the wind conversion system is a unacceptable risk.
   To compare the systems in terms of robustness, the number of moving parts exposed to the environment and the sensitivity of the system to wear and tear are taken into account. Soft sails and the lines to control them are generally found to be less robust, as the underlying materials are highly sensitive to wear from external loading which shortens the lifetime of this system at sea. Because a Flettner rotor spins as a whole, Gyroscopic effects will provide a resistance to roll and pitch motions of the vessel providing additional loads on the bearings present in the system. The Turbosail uses a ventilator for boundary layer control which has a high number of moving objects, but as this ventilator is placed at the bottom inside the structure, it is less exposed to the environment and therefore more robust than Flettner rotors. Wingsails consistist of a solid and stiff wing-shaped structure, providing excellent capabilities to withstand harsh conditions at sea.

3. Scalability
   For significant contribution to the ship's propulsion a maximum thrust is desirable. This requires a larger wind converter than any wind converters currently in use. Thus, a high scalability of the system is a requisite. The simplicity of the Soft Sail systems and limited construction weight makes them easily scalable, except for the Kite, where an increase in size and weight will make the system uncontrollable. Just as soft sails, Wingsails are easily scalable in terms of number of masts and sail size, the only challenge can be maintaining stiffness in the construction. Flettner rotors are limited in scalability due to bigger momental forces resulting from the gyroscopic effect. A problem which can arise in the scaling of Turbosails is associated with the equal distribution of suction force.

4. OPEX
   It is desirable that the system is available at a low cost. The financial performance of the system will be based on OPEX and CAPEX estimations. The OPEX will be mostly related to maintanance costs and the cost op running the system. The Kite is a good example op a high OPEX system as it needs active control and it consists of soft fabric and connecting lines fully exposed to the environmental conditions which leads to high maintenance costs. The OPEX of an active wind conversion is usually higher than for a passive system due to the energy that the active system consumes. Active sails tend to have more moving part therefore requiring additional maintenance compared to passive systems.

5. Operability
   It is desirable that the system can deliver positive thrust in a wide range of wind conditions in terms of both angle and wind velocity window. Options to decrease the induced forces of a sail will increase operability. A Kite can be lowered during severe storm conditions and the sail area of a Dyna rig can be reduced. The wind angle for which a system can produce positive thrust is the other criterion to measure operability. A Kite has limited drift force creating capabilities, limiting the operable angle to running

wind conditions. The Dyna rig has a large angle window and can be decreased in size when needed, the Turbosail has the largest angle window and the created force can be controlled by adjusting the suction power of the ventilator.

6. Controllability
   High simplicity of operation of the system is desirable. Preferably, the system is operable from the bridge of the ship. The Square rig and Bermuda rig both need separate control for the different sail areas. The Dyna rig, Aero rig and Wingsail are only controlled by rotation of the attachment point of the vessel. The only controlled parameter for the Flettner rotors is the rotational velocity, making it the easiest system to control. Turbosails have both the orientation and suction force that need to be managed.

7. CAPEX
   The Capital Expenditure (CAPEX) in this context is defined as the investment needed to install a system onboard. Simplicity of a system and availability on the market are requirements for a high rating. Therefore, the Square rig, Dyna rig and Aero rig all have a high ratings in terms of CAPEX. The Kite is still in its test phase and multiple systems are needed to be installed to produce forces equal to the other systems with a much smaller area. Active components will increase the cost of a system resulting in lower ratings for the Turbosail and Flettner rotor in terms of CAPEX.

8. Maturity
   High maturity of the system is desirable, as a mature stage of development of the system comes with increased knowledge about the behavior and performance of the system. This means more data about the performance is available enabling better performance prediction for a wind-assisted tow simulation designed with such a system. We base the rating on the available amount of information from scientific sources and the number of operative examples of the system sailing around.

For the MCA anaysis, the systems are provided with a rating for each of the eight criteria. Each criterion is provided a weight factor. The propulsive performance has been assigned a total weight factor of 10, of which a factor 5 is assigned to adjust the criterion's scale from 1.6 to 4.86 to the scale of the other criteria. An additional factor 5 is provided because the propulsive performance is the most important criterion in determining the feasibility of the Sailing Tug-Thialf combination, as when aerodynamic properties proves to be sufficient other wind conversion systems can easily be implemented based on reconsidered weight factors. The remaining weight factors and system ratings were determined in consultation with internal HMC sources. Subsequently, the relative performance of each of the wind conversion systems have been graded from 0 (least favorable) to 10 (most favorable) for each of the eight criteria. The results of the comparison are presented in Table 2.2. From Table 2.2 it can be derived that the Turbosail system obtains the highest total score of 149.6, indicating that this wind conversion system will most likely lead to a feasible Sailing Tug design. We therefore choose to use the Turbosail system for the design of the Sailing Tug.

Criteria	Weight	Square rig	Bermuda rig	Dyna rig	Aero rig	Kite	Wingsail	Flettner rotor	Turbosail
1. Propulsive Performance*	10	1.60	1.65	2.12	2.53	-	3.00	3.41	4.86
Maximum lift coeff.	-	1.6	1.5	1.8	1.9	-	2.1	7.5	6.8
Associated drag coeff.	-	1	0.91	0.85	0.75	-	0.7	2.2	1.4
2. Robustness	3	3	4	3	4	3	9	7	8
3. Scalability	3	9	9	8	8	2	8	6	7
4. OPEX	3	5	8	7	7	2	10	4	4
5. Operability	3	3	4	9	7	1	3	7	9
6. Controlability	2	2	4	9	9	2	7	10	6
7. CAPEX	1	9	9	7	6	1	3	3	2
8. Maturity	1	10	9	7	4	2	7	5	3
Total**	-	**99.0**	**117.5**	**134.2**	**131.3**	**58.0**	**144.0**	**134.1**	**149.6**

Notes: *Propulsive Performance equals Maximum lift coefficient divided by Associated drag coefficient.
**Total score is equal to the sum of the weight factor times the given score per criterion.

Table 2.2: Multi-Criteria Analysis of the Wind Conversion Systems

2.3. The Sailing Tug Design

Creating a purpose-built sailing tug requires an enormous investment, and especially in the current competitive offshore market this is undesirable. Therefore, we choose to use an existing discarded Panamax vessel and convert it into a sailing tug which is an alternative more economic option.

There are two reasons to use the specific Panamax bulk carrier as a basis for the Sailing Tug. The first reason is that previous research for HMC indicated that a discarded Panamax can serve as a floating breakwater (Smulders, 2017). Thus, combining the concept of a floating breakwater with a sailing tug gives an additional economic advantage for using discarded Panamax vessels. The second reason is the recent widening of the Panama-canal [1] which enables the passing of larger vessels besides the Panamax vessels, such that the expected prices for discarded Panamax vessels have decreased.

The design of the Sailing Tug, the converted Panamax vessel, consists of three parts: the specifications of the specific Panamax hull that is selected, the Turbosail setup in terms of number and dimensions of the sails, and finally the positioning of the sails on the deck.

2.3.1. Panamax Specifications

The Panamax Leda C, a 2011 80000 DWT bulk carrier with IMO 9583768, as depicted in Figure 2.2 will be used as a test-case for the basis of the Sailing Tug conversion[2]. The specifications of the vessel are provided in Table 2.3. The reason this particular vessel is selected, is the availability of SketchUp 3D drawings as displayed in Figure 2.3 which provide precise specifications on the stability, surface areas and dimensions of the vessel.

Vessel name	Leda C
Length	229 [m]
Beam	32.24 [m]
Height	15.99 [m]
Average draft	11.2 [m]
Freeboard	4.59 [m]
Dead weight tonnage	81526 [tonne]
Gross tonnage	44600
Maximum speed	18.6 [knots]
Average speed	9.5 [knots]
Installed power	9470 [kW]
RPM	91
Propeller diameter	6.4 [m]
Rudder span	10 [m]
Rudder height	7 [m]

Table 2.3: Panamax specifications

[1] http://micanaldepanama.com/expansion/
[2] http://www.shipspotting.com/photos/middle/6/6/4/1764466.jpg

Figure 2.2: Panamax test-case

Figure 2.3: Panamax test-case SketchUp

2.3.2. Conversion Setup

In taking the Panamax Leda C hull for the basis of the design, the vessel will be converted into the Sailing Tug by installing Turbosails on deck. It is assumed that a ballast system is present which can be used to keep the transit draft of the Sailing Tug equal to the 11.2 meters of the original Panamax. The goal is to create a setup that maximizes the force in the sailing direction, such that a maximum tow force is yielded. Employing the Panamax bulk carrier for tugging purposes introduces two new loads on the vessel. First, there is the load of the towed vessel through the towline, in this case the Thialf. Second, there is the propulsive power provided by the sails. The force provided by the Turbosails will have a less controllable direction and magnitude than force provided by the propeller and the point of engagement will differ.

Theoretically, the number and dimensions of the sails installed can be scaled up until the magnitude of the force is as desired. There are two possible limiting factors on the surface area and engagement point of the sails that can be placed on the hull,

- The heeling moment provided by the sails will be too large to be compensated by the restoring moment (M_r) of the Panamax hull.
- The windforce in vessel y-direction will be larger than the maximum achievable leeward resistance of the Panamax hull under a drift angle.

Therefore, the restoring moment of the Panamax hull at a maximum allowable heeling angle and the maximum achievable leeward resistance need to be calculated to determine the sail design. Since the leeward resistance largely depends on sailing velocity, this will be taken into consideration as a boundary condition that will be checked during simulation of the setup. As such, we only use the restoring moment of the Panamax hull to determine the maximum sail area and the resulting initial design of the sails.

The maximum allowable sail area will be determined for a sailing case and not under survival conditions. The force provided by the sails can be controlled by the aspiration power as well

as the sail angle. With the sails trimmed to the setting that yields minimal force, the force coefficient declines by approximately a factor 10 (J.A. Cousteau, 1985). Assumed is that the Panamax hull restoring moment is sufficient to compensate the forces of the sails in survival setting.

To determine the maximum sail area for the sailing case, we are looking for an equilibrium in roll moments at the maximum allowable heeling angle of 15°(Brockett, 1964), which is below the deck immersion angle of 15.89°. At this 15°heeling angle the rudder is still fully submerged as illustrated in Figure 2.4.

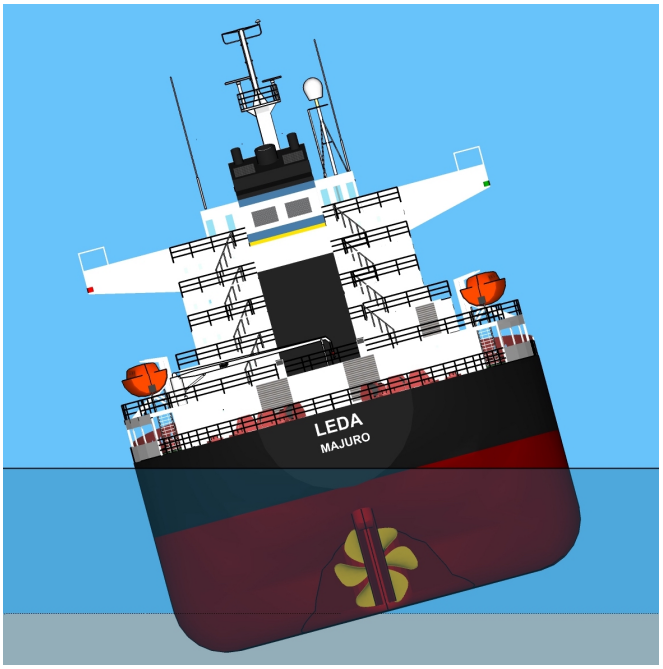

Figure 2.4: Panamax under 15 °heel angle at a 11.2m draft

Thus, we calculate the maximum restoring moment M_r at the point at which it is in equilibrium with the external heeling moment M_e of a maximum 15°heeling angle accordingly,

$$M_r = M_e, \tag{2.1}$$

with M_r the restoring moment and M_e the external heeling moment, in this case the wind force on the sails.

The restoring moment M_r is determined using the approximating formulae as provided by Journée et al. (2000),

$$M_r = \rho * g * \nabla * \overline{GZ} \tag{2.2}$$

In which the stability lever arm $\overline{GZ}$ can be written as,

$$\overline{GZ} = \overline{GN_\phi} * sin(\phi) \tag{2.3}$$

where the $\overline{GN_\phi}$ can be defined as a function of the keel-buoyency distance, $\overline{KB}$, the buoyency-metacentre distance under a heel angle, $\overline{BN_\phi}$, and the keel-centre of gravity distance, $\overline{KG}$,

$$\overline{GN_\phi} = \overline{KB} + \overline{BN_\phi} - \overline{KG} \tag{2.4}$$

under the assumption of a wall-sided vessel, this can be re-written as,

$$\overline{GN_\phi} = \overline{GM} + \frac{1}{2}\overline{BM} * tan^2(\phi) \tag{2.5}$$

with $\overline{GM}$ the actual metacentre height and $\overline{BM}$ the distance between the center of buoyency and the metacentre.
$\overline{GM}$ can be found by means of an inclination test, but the results of such a test are not available for the considered Panamax vessel. There are methods to get an estimation of $\overline{GM}$ through approximation formulae, for example the method of Posdunine and Lackenby (Bertram and Schneekluth, 1998), which is recommended for vessels with a midship coefficient $C_m > 0.9$, which is the case for the Panamax vessel. Thus, by Posdunine and Lackenby,

$$\overline{GM} = \overline{KB} + \overline{BM} - \overline{KG}, \tag{2.6}$$

where

$$\overline{KB} = \frac{T}{1 + C_b}, \tag{2.7}$$

and

$$\overline{BM} = \frac{I_t}{\nabla}, \tag{2.8}$$

and

$$\overline{KG} = 8.16. \tag{2.9}$$

The draft T, the block coefficient C_b, the waterplane moment of inertia I_t, $\overline{KB}$ and $\overline{KG}$ are estimated using the 3D drawings of the Panamax vessel.
Thus, we can substitute the parameters into equation 2.6 to find the the maximum restoring moment at a 15°heeling angle to be,

$$M_r = 594492kNm. \tag{2.10}$$

Accordingly, an initial sail layout can be designed based on the following assumptions for parameter values that satisfy the maximum restoring moment:

- Mast height = 80m,
- Arm length = 40m,
- Turbosail aspect ratio = 1/6 (J.A. Cousteau, 1985),
- $v_{w,max}$ = 44 m/s (H.W. van den Brink, 2017),
- Maximum wind coefficient in y-direction C_y = 2,
- Density of air ρ = 1.293.

Such that the surface area of each sail A_{sail} can be calculated as follows,

$$F_{y_{max}} = \frac{M_e}{Armlength} = 14862kN, \tag{2.11}$$

with the total surface area equal to,

$$A_{sail,total} = \frac{F_{y_{max}}}{\frac{1}{2} * \rho * v_{w,max}^2 * C_y} = 5937m^2, \tag{2.12}$$

dividing by the number of sails to find the area for each sail,

$$A_{sail} = \frac{A_{sail}}{6} = 990m^2. \tag{2.13}$$

The initial design of the Sailing Tug with the selected parameters has six Turbosails each with a surface area of $990m^2$ equally distributed on deck, as is illustrated in Figure 2.5.

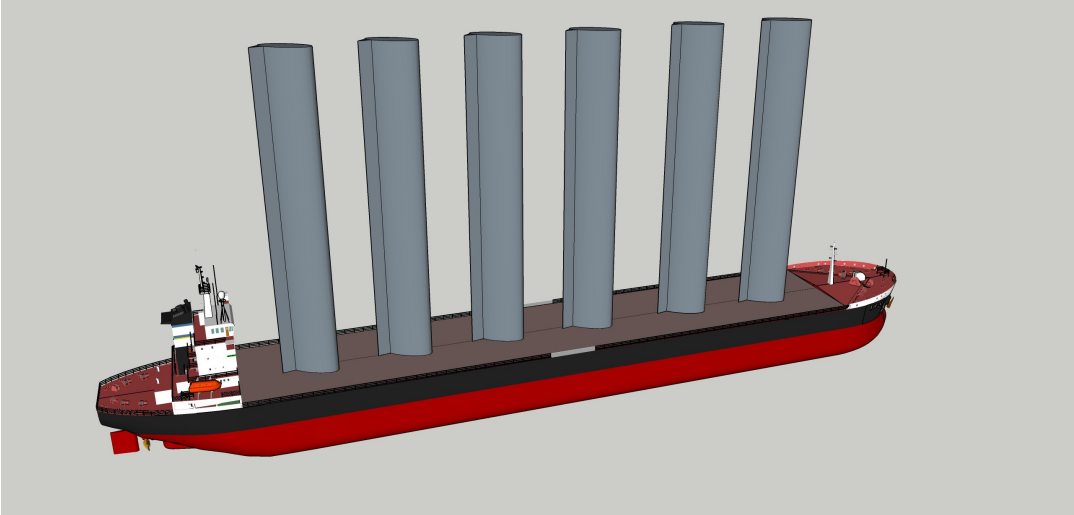

Figure 2.5: Initial design of the Sailing Tug, a wind-assisted Panamax

2.3.3. Positioning of the Sails

Besides a heeling moment exerted on the Panamax hull by the sails on-deck, an additional yaw moment may be introduced as a result of the wind force. The magnitude of the yaw moment depends on the positioning of the sails, as illustrated in Figure 2.6 which depicts two situations with different sail positions.

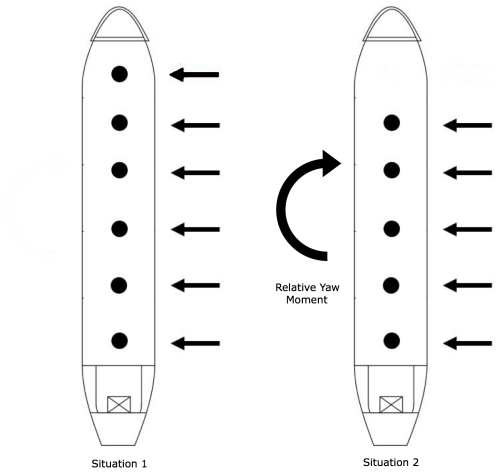

Figure 2.6: Relative yaw-moment introduced based on sail positioning

Figure 2.6 displays that in situation 2 a relative yaw moment around the vessel's geometric center is present compared to situation 1 where the sails are placed along the center-line of the vessel and are evenly distributed along the geometric center of the ship. Initial results indicated that large rudder angles are required to provide a sufficient drift angle to withstand the leeward force. By placing the sails such that they are more heavily distributed along the center-line towards the vessel's aft, the additional relative yaw moment introduced can partly inhibit the needed moment to create the necessary drift angle.

To further test the effect of the longitudinal distribution of the sails on the ship, the sail positioning will be tested with the required rudder angles needed for a sufficient drift angle.

3

Bodies and Forces in wind-assisted Towing

To assess the performance of the wind-assisted tow operation of the Sailing Tug-Thialf combination, the goal is to determine a static force balance for every combination of input conditions on the system. The system consists of the Thialf and the Sailing Tug combined through towlines.

In this chapter, an overview of the bodies and forces working on the system is provided. Furthermore, the sources used for the approximation of the forces will be described. These forces will serve as inputs for the Velocity Prediction Program, described in chapter 4

3.1. Forces Acting on the Thialf Under Tow

The goal of the wind-assisted Sailing Tug-Thialf configuration is to sail without using the thrusters installed on the Thialf. As a result, the Thialf will act as a passive box and will only experience loading from from a) Environmental loading and b) the Towline force, illustrated in Figure 3.1.

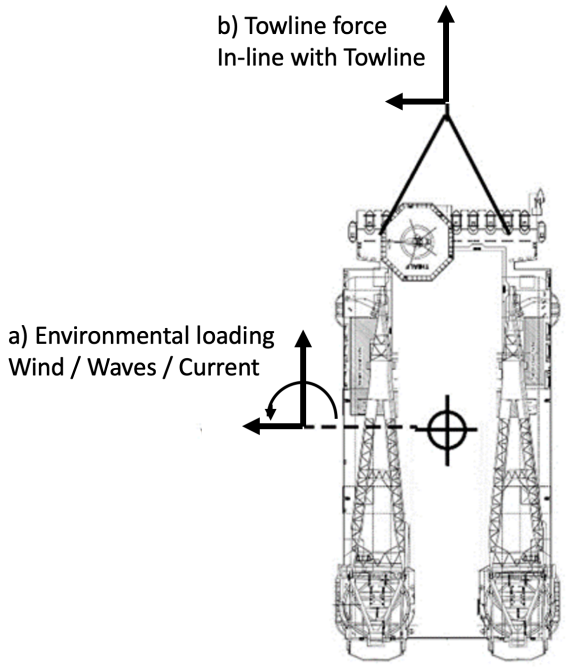

Figure 3.1: Overview of forces exerted on the Thialf

3.1.1. Environmental Loading (a)

The environment exerts loading on the vessel in three ways:

Hydrodynamic Loading

The hydrodynamic loading on the underwater body is a result of the velocity of the water around the hull. This velocity results from the presence of current and the vessel's movement through the water. Since the hydrodynamic loading plays an important role in position-keeping during HMC's heavy lift activities, the behavior of the Thialf is well researched. Hydrodynamic loading coefficients are determined by CFD analyses as well as scale model tests. The outcomes are documented as coefficients for force in the x-direction, y-direction and a moment around the geometric centre per 15°angle of attack to simplify calculations. These coefficients will be employed for estimating the hydrodynamic loading on the Thialf.

Wind Loading

Wind yields aerodynamic forces. On the sails of the Panamax these aerodynamic forces serve as propulsion, on the Thialf these aerodynamic forces provide resistance. At transit draft ($T = 12m$) the deck of the Thialf is located 37.5 meters above the waterline. This, in addition to the the cranes and accommodation present on deck cause a large area of the vessel to be exposed to wind, resulting in resistance.

The total force and moment exerted on the Thialf due to wind exposure is partly of viscous origin (pressure drag) and partly due to potential effects (lift force). For the Thialf, the wind load is regarded as independent of the Reynolds number and proportional to the square of the wind velocity. Coefficients for wind load prediction are available within HMC for the Thialf in the same form as the hydrodynamic loading coefficients. These coefficients will be employed for estimating the wind loading on the Thialf.

Wave Loading

Since the goal of this research is to find a static force balance, dynamic forces exerted on the Thialf from waves at wave-frequency are ignored. The second order wave drift forces present a mean static load on the vessel and will be taken into account. Within HMC, the quadratic transfer functions of the Thialf have been documented, as such the mean wave load using the Pierson-Moskowitz (PM) wave Spectrum can be calculated, a common assumption for open-sea wave conditions.

The wave load is approximated using coefficients that depend on significant wave height, encounter frequency and angle of attack and are determined with the boundary integral equations method at zero speed, using WAMIT. The results at 15°angle of attack, for encounter frequencies from 4 to 18 seconds, are available in tables which will serve as input for the wave drift force approximation in this research.

An overview of the wave coefficients for the Thialf is provided in Appendix B.

It is important to note is that the encounter frequency, and thus the encounter period, changes due to the movement of the vessel. Because ocean waves are approximated as harmonic waves in WAMIT, the change in wave drift forces on the vessel can be accounted for by the following formula provided by Journee (2002),

$$\omega_e = \omega - (\omega^2/g) * V * cos(\mu) \tag{3.1}$$

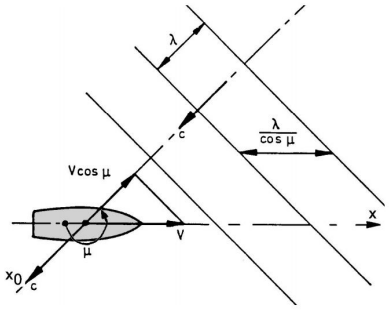

Figure 3.2: Encounter frequency under angle

Determining the wave drift force based on this encounter frequency while using the wave drift coefficients for zero vessel velocity is a simplification and can result in deviation from the actual wave drift force.

The horizontal movement of the system will not influence the height of the incoming waves. Under the WAMIT assumption of harmonic waves, the shape of low frequency and high frequency waves will both be sinusoidal, and therefore be constant as well. What does change are the assumed orbital velocities in the wave. Within WAMIT, a relationship between wavelength and orbital velocities is assumed, [1] a vessel velocity will not have an effect on this orbital velocity. When approximating the wave drift force using the coefficients for the adjusted encounter frequency, the assumed orbital velocities belonging to the encounter frequency will be different from the orbital velocities in the wave at the actual wave frequency. For example, when encountering head waves at a positive vessel velocity, the encounter frequency will be higher than the actual wave frequency. As a result, the orbital velocities of a higher frequency wave will be assumed, resulting in a higher velocity potential and therefore a higher wave drift force. Due to the low transit velocity during a tow operation, this effect is not taken into account.

[1] $www.wamit.com/manualupdate/history/V70_manual_old.pdf$

3.1.2. Towline Force (b)

During a tow operation, the wires in the bridle-towline combination will act as springs and the force from the towline will depend on the relative distance between the two vessels. The wires will provide tension forces in line with their direction as the lines will be slack otherwise. Because the aim of this research is to achieve a static force balance, the dynamic spring effect will not be included.

To mimic the static behavior of the tow wires, they are implemented as massless bodies, connected with pin-joints on both ends and with a maximum distance between both ends, but no minimum to incorporate slack. Under this implementation, the force on each side depends solely on the difference in the sum of forces acting on the wind-assisted Panamax and the Thialf. There will be no forces perpendicular to the towline an the force from the towline acting on either vessels is equal but opposite in sign.

The towline force is not an external force on the system and is therefore not calculated as part of the forces working on the system. Instead, the towline force , $F_{towline}$, is calculated manually for verification purposes as follows,

$$F_{towline} = \sqrt{(\sum F_{T,X} - \sum F_{P,X})^2 + (\sum F_{T,Y} - \sum F_{P,Y})^2}. \tag{3.2}$$

With $F_{T,X}$ and $F_{T,Y}$ the forces on the Thialf and $F_{P,X}$ and $F_{P,Y}$ the forces on the Panamax.

3.2. Forces Acting on the Panamax

The wind-assisted Panamax experiences loading from the environment and a towline force. Apart from these loadings, three more forces are present: A propulsive force from the propeller, a rudder force and the force provided by the six Turbosails present on deck. The forces exerted on the Panamax are illustrated in Figure 3.3.

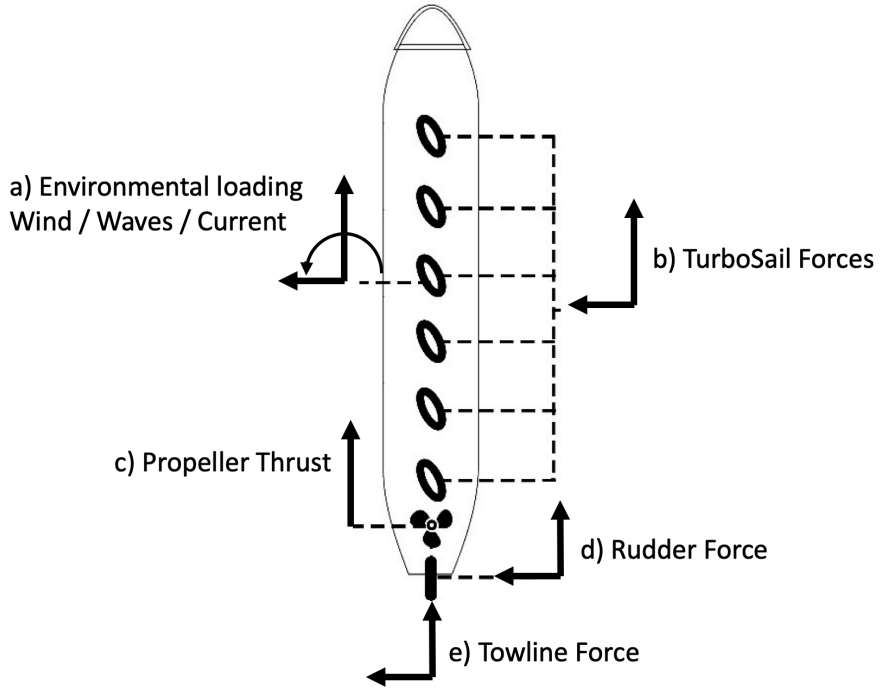

Figure 3.3: Forces acting on the Panamax: a) environmental forces and moments b) TurboSail forces c) Propeller thrust d) Rudder forces e) Towline force

3.2.1. Environmental Loading (a)

The behaviour of the Thialf under environmental loading is well-documented within HMC. However, for the chosen Panamax basis in this research this is not the case. Wind and current design coefficients and calculation procedures have been developed by the Oil Companies International Marine Forum (OCIMF, 1994) and is the force estimation method recommended by Lloyd Register (Vroegrijk, 2017). These coefficients are non-dimensionalized such that they apply to a wide variety of Very Large Crude Carriers (VLCCs). Although the Panamax basis used for the Sailing Tug is a bulk carrier, the OCIMF coefficients for VLCCs are the most suitable 2D input available to approximate the wind and current load predictions for our model.

Wave Loading

For wave load approximation, the OCIMF tables only provide longitudinal forces for waves coming in at the bow of the vessel in relatively shallow water, $WD/t = 2$. Under the wind-assisted Panamax transit conditions these coefficient do not provide a correct representation of of the wave drift forces. Within HMC, the wave drift force for the mono-hull vessel Aegir are available in the same form as the Thialf wave load coefficients. The dimensions of the Aegir and Panamax basis show large similarities: the Aegir length equals 212m and the Panamax length 229m; the Aegir width equals 46.2m and the Panamax width 33.6m. Therefore, the Aegir PM-spectrum wave drift force coefficients will be used in this research to determine the wave loadings on the Panamax.

3.2.2. Turbosails Forces (b)

The force contribution from the six Turbosails present on deck is the most distinctive factor of the vessel's force balance as compared to the conventional tow operation. For a conventional vessel driven by a propeller, the thrust is mainly directed in the direction of the vessel heading. In case of propulsion by sails, the direction of the force is less controllable. This results in a relatively large leeward force contribution under most wind angles of attack. To counteract this leeward force the wind-assisted Panamax must adopt a drift angle.

Nelissen and Mao (2016) used the lift and drag coefficients from J.A. Cousteau (1985) to determine the optimal sail angle to yield the maximum propulsive force in the application to a cargo vessel. With the drag force component always being in line with the wind and the lift force perpendicular to the wind, it is beneficial to maximize the drag force when the wind is coming from behind where for beam reach conditions the lift yield should be maximized. With the global global wind coefficients provided by Nelissen and Mao (2016), C_X and C_Y, the wind force can be determined in the moving coordinate system independent of the vessel heading.

The global wind force coefficients C_X and C_Y determined by Nelissen and Mao (2016), as well as the original Cousteau coefficients are provided in Appendix D.

3.2.3. Propeller Thrust (c)

To determine the maximum sailing velocity, the propeller power is fixed at its Maximum Continuous Rating (MCR). The delivered thrust at various advance speeds and iflow angles relies on a variety of vessel specifications and hull parameters. In the conceptual stage of this research, these parameters are not yet available such that advanced model testing or CFD simulation are required. Since this level of detail will not contribute to the proof of concept of the wind-assisted Tow operation, another method to determine the on-speed thrust will be used.

Kinaci et al. (2013) investigated the propeller performance using a benchmark Duisburg Test Case (DTC) ship with RANSE. Although the vessel used in the research by Kinaci et al. (2013) differs in dimensions from the Panamax vessel in this research, the propeller and hull shape show large similarities. It is therefore assumed that the propeller thrust (K_t) values from Kinaci et al. (2013) provide a better estimation than open water characteristics. Since the advance ratio and thrust resulting from the K_t values show a relative linear relation, see figure 3.4, the thrust, $F_{propeller}$ is estimated as:

$$F_{propeller} = 750 - (J * 600), \tag{3.3}$$

where the advance ratio J is defined as,

$$J = \frac{V_i}{n * D_p}, \tag{3.4}$$

with inflow velocity V_i, Propeller RPM n and propeller diameter D_p.

The maximum thrust, attained when advance ratio $J = 0$, for a 9470 kW bulk carrier is determined to be 750 kN (Żelazny, 2015). An overview of the K_T values at different values of J is provided in Figure 3.4, for a numerical overview see Table C.1 in Appendix C.

The inflow angle is expected to have an influence on the propeller performance, especially since the wind-assisted Panamax is sailing under a drift angle more often when compared to a regular Panamax.Drenthe et al. (2016) determined that the influence of inflow angles up to 10°is smaller than 6,99% in open water tests. Since there is also a straightening effect of the vessel's hull, the effect of inflow under and angle is neglected in this research.

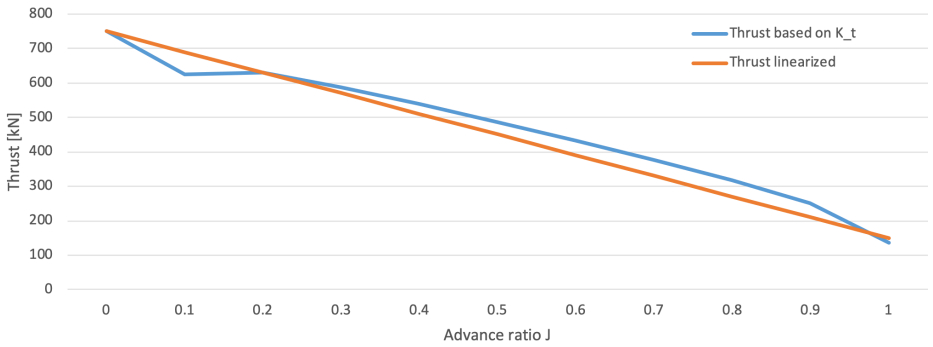

Figure 3.4: Panamax propeller thrust based on K_t (Żelazny, 2015) and linearization

3.2.4. Rudder Forces (d)

The rudder creates the yaw moment that yields the sufficient drift angle. The rudder side force $F_{r,y}$ acting on the ship aft creates the yawing moment. The penalty is the rudder induced drag $F_{r,x}$.

The forces inhibited by the rudder angle can be approximated by the formula as used by Liu et al. (2015). The rudder normal force is the force perpendicular to the rudder face. Rudder drag at zero rudder angle is assumed to be small and incorporated in the current resisted coefficients provided by OCIMF (1994). The heel angle of the Panamax will influence the generated rudder side force. When only considering the change in direction resulting from a heel angle, the rudder side force will decrease by a factor $cos(15°) = 0.966$. To gain more insight in the real effect of the heel angle, more detailed investigation is necessary. At this stage of the research the effect of a heel angle on the rudder performance is neglected. Thus, we determine the rudder normal force according to Liu et al. (2015).

$$F_N = 0.5 * \rho_w * A_R * U_R^2 * C_N, \tag{3.5}$$

where the rudder normal force coefficient C_N is determined with the empirical method of Fujii (1960),

$$C_N = \frac{6.13 * \Lambda}{\Lambda + 2.25} * sin(\alpha_R), \tag{3.6}$$

where Λ is the rudder aspect ratio and α_R the effective inflow angle of attack.

The rudder stall angle is assumed to be around 25°, measured relative to the incoming flow. For larger effective rudder angles boundary layer separation will occur. Rudder drag will increase while the lift component will vanish. Rudder angles beyond the rudder stall angle are not an effective measure to control the vessel heading (Fujii, 1960).

3.2.5. Towline Force (e)

As illustrated in section 3.1.2, the towline force acting on the Panamax aft is equal to the force at the bridle plate but opposite in direction.

$$F_{towline,Panamax} = -F_{towline,bridle}. \tag{3.7}$$

4

Velocity Prediction Program

With the bodies and forces present in the system of the Sailing Tug-Thialf combination introduced in the previous chapter, the next step is to construct a model, a Velocity Prediction Program (VPP). The VPP determines a force and moment equilibrium position of the system such that the maximum sailing velocity of the Sailing Tug-Thialf can be predicted.

The following chapter provides a description of this simulation environment which can provide the equilibrium parameters for every combination of environmental conditions.
This includes a description of the simulation block diagram, the program tools employed to construct the environment and the implementation of the input-variables.

All vessel force coefficients are provided in the form of tables as presented in Appendix B to D, making it impossible to solve the balance in an analytical way. Therefore, an iterative solver is designed.

The complete simulation is built in Python at the request of HMC as Python code tends to be more compact and readable than Matlab. Being open source gives it a wider variety in available toolboxes and in terms of cost competitiveness, Python is free.

Furthermore, Pymunk is used to provide the necessary 2D multibody physics. For the visualization a package called Pygame is used, a package frequently used to create simple games.

4.1. Balance Solving Strategy

To predict the maximum sailing velocity of a vessel, a model known as a velocity prediction program (VPP) is constructed based on the principles of Newton's second law:

"For any body which is not accelerating, the sum of forces in each coordinate direction, and the sum of moments around each coordinate axis must be zero".

The goal of the VPP model is to provide this force and moment equilibrium for the Sailing Tug-Thialf system. The distinctive property of a wind-assisted tow VVP is the fact that there are two bodies which can rotate independently and influence each other by forces transferred through the towline connecting the two bodies. To solve the force equilibrium, two controllable parameters are selected. First, the sailing velocity is selected, which is the dominant parameter for force-balance in the sailing direction. The second parameter is the rudder angle which is the main measure to control the Panamax drift angle and thus the force balance perpendicular to the sailing direction.

Environmental input velocities are defined as earth-fixed velocities and forces working on the two vessels are declared in a vessel-specific coordinate system. Before a balance can be searched for, a coordinate system needs to be selected.

4.2. Moving Coordinate System

To solve the balance equation, a moving coordinate system will be employed. This moving coordinate system will travel with the velocity of the Panamax-Thialf combination. Adjustment of the velocity of the vessels and thus the coordinate system will influence all forces within it. The X-axis will be oriented in the direction of travel and will be independent of both vessels' drift angles β_T and β_P, illustrated in Figure 2.

To solve the force equilibrium in the moving coordinate system, the environmental velocities and directions within the coordinate system are needed. These velocities and angles depends on both the earth fixed condition and the velocity and orientation of the moving reference frame, the so-called apparent velocities and directions.

The wide variety of independent forces on both vessels present in the moving coordinate system makes it impossible to find the balance condition in an analytical way. Therefore, the proposed method to solve the force equilibrium within the moving coordinate system is to run a time domain simulation which will converge to a steady-state of the system providing the balance-condition within the moving coordinate system. This way the moving coordinate velocity where a force balance is achieved, will be the maximum sailing velocity.

4.2.1. Rotation Matrix

Forces calculated using the vessel coefficients are defined in the vessel-specific coordinate system, the actual balance is solved in the moving reference frame as described above, and some output of the model is checked for verification back in the vessel-specific system. Forces can be converted to the equivalent ship-specific coordinate system using the following rotation matrix R,

$$R = \begin{bmatrix} cos(\beta) & -sin(\beta) \\ sin(\beta) & cos(\beta) \end{bmatrix}$$

To convert global forces F_X and F_y to ship-specific coordinate systems the inverse of the rotation should be used, as illustrated in Figure 2.

$$F_X = cos(\beta) * F_x - sin(\beta) * F_y \tag{4.1}$$

$$F_Y = sin(\beta) * F_x + cos(\beta) * F_y. \tag{4.2}$$

4.3. Model Block Diagram

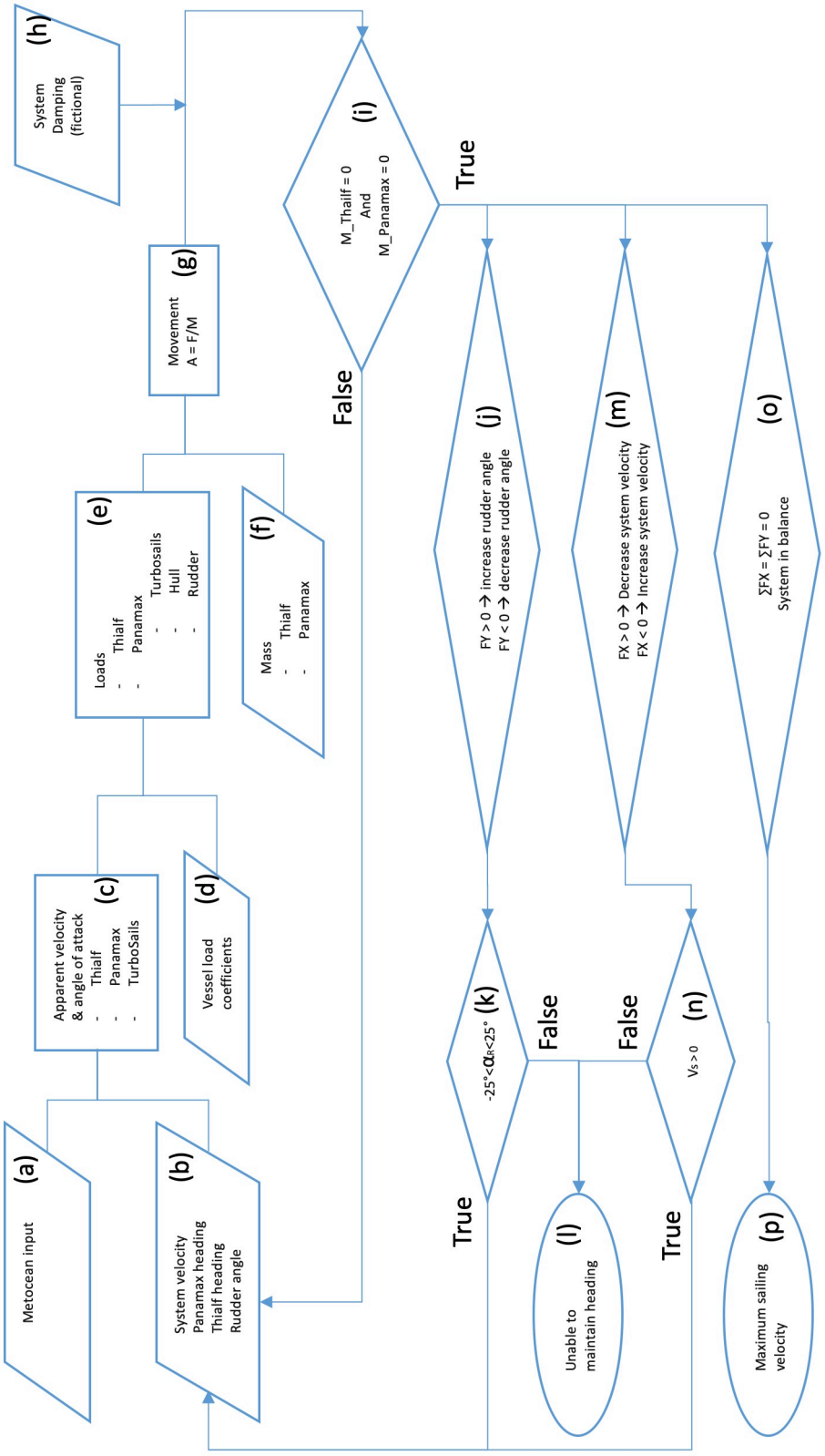

Figure 4.1: Model block diagram

(a) Metocean Input
At this block the user-defined input parameters are implemented, consisting of:

- Wind: Direction and velocity
- Current: Direction and velocity
- Waves: Direction, significant height and frequency

Based on Figure 2, directions are declared as “coming from” relative to the orientation of the moving reference frame. Velocity is defined as the earth-fixed velocity. The wind input-velocity is defined as the V_{10}, the wind velocity at a 10 meter height, this is the required input for the used OCIMF and HMC coefficients. For the Turbosails this presents a conservative approach of the generated forces since the lift- and drag-coefficients are determined for a smaller sail. Wind velocity has an exponential relationship with height, so the actual sail-generated forces will most likely be higher.

For the simulations used to create polar plots, the global current velocity is fixed on 0 m/s, such that the flow around both vessel hulls depend solely on the sailing velocity. The option can be used to check the system performance for cases where current is present.

(b) System Settings
In this stage the following system-specific parameters are determined:

- Moving coordinate system velocity,
- Panamax orientation,
- Thialf orientation,
- Rudder angle,

For the start of the simulation the following set of predefined parameters is selected:

- Moving coordinate system velocity: 6 knots = 3.09 m/s,
- Panamax orientation: 0°,
- Thialf orientation: 0°,
- Rudder angle: 0°,

with the Panamax and Thialf in line on the X-axis of the moving coordinate system. The system start velocity of 6 knots is based on the average conventional transit velocity. The closer the starting velocity is to the final balance velocity, the fewer iterations are needed to find this balance.

(c) Apparent Velocity and Angle of Attack

The loads resulting from environmental conditions do not directly relate to the global defined conditions. For the load calculation, the velocities and angles as experienced on the vessel are needed, the so-called apparent velocities and angles.

This apparent velocity V_a and angle of attack α can be calculated with the moving coordinate system velocity, $V_{sailing}$, the earth fixed metocean input velocities, V_{true} and the true direction with respect to the moving coordinate system, α_{true}. To get the angle of attack α on a vessel for load calculation, the specific vessel drift angle β should be subtracted from the apparent direction within the moving reference frame, γ.

$$V_a = \sqrt{V_{true}^2 + V_{sailing}^2 + 2 * V_{true} * V_{sailing} * cos(\alpha_{true})} \tag{4.3}$$

$$\gamma = cos^{-1}(\frac{V_{true} * cos(\alpha_{true}) + V_{sailing}}{V_a}) \tag{4.4}$$

$$\alpha = \gamma - \beta, \tag{4.5}$$

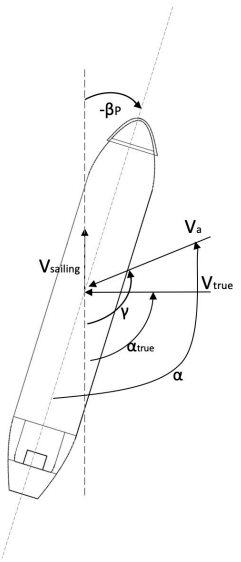

Figure 4.2: Panamax angle overview

(d) Vessel Load Coefficients Import

The vessel load coefficients are imported from csv text files into arrays. As the in-house HMC tables only provide coefficients per 15 °, the arrays are interpolated to provide the coefficient for every intermediate angle.

The OCIMF coefficients which are used for the Panamax loading are provided per 10 °, these are interpolated in the same manner. To smooth out sharp peaks in the vessel loading coefficients, a cubic spline interpolation is used.

An overview of the Thialf and Panamax load coefficients can be found in appendix B and appendix C, respectively.

(e) Load Calculation

Environmental loading from wind and current on the Thialf are dependent on the apparent velocity and angle of attack, wave loading depends on the angle of attack, encounter frequency is determined as in equation 3.1 and wave height is defined in the input.

The OCIMF loading coefficients are non-demensionalized such that they apply on a wider variety of vessel dimensions. To apply the coefficients specifically for the Panamax case, the coefficients need to be multiplied with water density ρ_w, transverse underwater area A_T, longitudinal area A_L and the length between perpendiculars L_{bp}.

Thus we can set up the following Load calculations for the Thialf and the Panamax,

Thialf:

$$F_{T,c,x} = C_{T,c,y}(\alpha_c) * V_{A,T}^2 \tag{4.6}$$

$$F_{T,c,y} = C_{T,c,x}(\alpha_c) * V_{A,T}^2 \tag{4.7}$$

$$M_{T,c,z} = C_{T,c,z}(\alpha_c) * V_{A,T}^2 \tag{4.8}$$

$$F_{T,w,x} = C_{T,w,y}(\alpha_w) * V_{A,T}^2 \tag{4.9}$$

$$F_{T,w,y} = C_{T,w,x}(\alpha_w) * V_{A,T}^2 \tag{4.10}$$

$$M_{T,w,z} = C_{T,w,z}(\alpha_w) * V_{A,T}^2 \tag{4.11}$$

$$F_{T,w,x} = C_{T,w,y}(\alpha_{wave}, T_e) * H_s^2 \tag{4.12}$$

$$F_{T,w,y} = C_{T,w,x}(\alpha_{wave}, T_e) * H_s^2 \tag{4.13}$$

$$M_{T,w,z} = C_{T,w,z}(\alpha_{wave}, T_e) * H_s^2 \tag{4.14}$$

Panamax:

$$F_{P,c,x} = 0.5 * C_{P,c,y}(\alpha) * \rho_w * V_A^2 * A_T \tag{4.15}$$

$$F_{P,c,y} = 0.5 * C_{P,c,x}(\alpha) * \rho_w * V_A^2 * A_L \tag{4.16}$$

$$M_{P,c,z} = 0.5 * C_{P,c,z}(\alpha) * \rho_w * V_A^2 * A_L * L_{BP} \tag{4.17}$$

$$F_{P,w,x} = 0.5 * C_{P,w,y}(\alpha_w) * \rho_a * *V_{A_w}^2 * A_T \tag{4.18}$$

$$F_{P,w,y} = 0.5 * C_{P,w,z}(\alpha_w) * \rho_a * V_{A_w}^2 * A_L \tag{4.19}$$

$$M_{P,w,z} = 0.5 * C_{P,w,z}(\alpha_w) * \rho_a * V_{A_w}^2 * A_L * L_{BP} \tag{4.20}$$

$$F_{T,w,x} = C_{P,w,y}(\alpha_{wave}, T_e) * H_s^2 \tag{4.21}$$

$$F_{T,w,y} = C_{P,w,x}(\alpha_{wave}, T_e) * H_s^2 \tag{4.22}$$

$$M_{T,w,z} = C_{P,w,z}(\alpha_{wave}, T_e) * H_s^2 \tag{4.23}$$

Turbosails:
The force provided by the Turbosails is declared in the moving coordinate system X, Y.
To enable application on the Panamax body, this force is converted to the Panamax vessel coordinate system,

$$F_{TurboSail,X} = \frac{1}{2} * \rho_a * A_S * C_Y(\alpha_w) * V_A^2 \tag{4.24}$$

$$F_{TurboSail,Y} = \frac{1}{2} * \rho_a * A_S * C_Y(\alpha_w) * V_A^2 \tag{4.25}$$

$$F_{TurboSail,x} = cos(\beta_P) * F_{TurboSail,Y} - sin(\beta_P) F_{TurboSail,X} \tag{4.26}$$

$$F_{TurboSail,y} = sin(\beta_P) * F_{TurboSail,Y} - cos(\beta_P) F_{TurboSail,X} \tag{4.27}$$

Rudder:
The rudder normal force is calculated by the formulae 3.5 and 3.6,

$$F_N = 0.5 * \rho * A_R * U_R^2 * C_N \tag{4.28}$$

$$C_N = \frac{6.13 * \Lambda}{\Lambda + 2.25} * sin(\alpha_R) \tag{4.29}$$

The rudder normal force is converted to the Panamax coordinate system and applied at the ships aft. δ is the rudder angle relative to the ship's centre line with the angle to starboard as positive direction.

$$F_{rudder,x_P} = F_N * sin(\delta) \tag{4.30}$$

$$F_{rudder,y_P} = F_N * cos(\delta) \tag{4.31}$$

Propeller
The propeller force is assumed to be always in line with the vessel's heading and the magnitude is determined by the formula below. The Propeller force is applied in x-direction to the Panamax body in front of the rudder.

$$F_{Propeller} = 750 - (J * 600) \tag{4.32}$$

(f) Vessel Masses
Vessel masses are fictional and chosen iteratively to provide a quick steady state. A negligible mass would result in a very large acceleration in the system leading to errors in the program.

(g) System Movement
The loads on the bodies will result in movement of the system by newtons second law:

$$Acceleration = \frac{Force}{Mass} \tag{4.33}$$

(h) System Damping
A fictional damping is applied as an undamped system will not converge. A critical damping is experimentally approximated by varying both vessel masses and the global damping in the system. Therefore the applied damping varies from case to case.

(i) Vessel Moment Check
After a certain amount of time the system will arrive at a point where the moments on both the Thialf and Panamax are zero. At this moment the orientation of both vessels will not change any more. There are still resulting forces in x and y direction present in the system.

(j) Rudder Adjustment
With the moment on the Thialf and Panamax in balance it is time to solve the force balance for the system. The rudder will be used to create a yaw-moment resulting in a drift angle. The rudder angle is adjusted until the point where the Panamax drift angle is sufficient to provide the needed leeward resistance for the complete system.

(k) Rudder Stall Angle
The ships transverse force provide by the rudder will increase until the angle between the inflow and rudder will arrive at the critical angle of attack or stall angle. At the point flow separation will occur and the lift effect will vanish.

(l) Unable to Maintain Heading
When the yaw-moment provided at the rudder stall angle is still not enough to create a sufficient drift angle the system will stop en display the message: ”unable to maintain heading”

(m) Sailing Velocity Adjustment
Simultaneous with the X-balance solving by adjusting the rudder angle, the Y-balance will be solved by varying the sailing velocity, which is equal to the moving coordinate system velocity Lowering the saling velocity will result in lower hydrodynamic drag on the hull (formula 5.4, 5.5, 5.13, 5.14) and influence the apparent angle and velocity in a positive way.

(n) Positive Velocity Check
When the is a negative force present at zero velocity the system will not be able to solve the force-balance and display the message: ”Unable to find balance”.

(o) System Balance Check
The final balance will be checked in the following three ways,

- The sum of forces in the moving coordinate system must equal zero,

$$\sum F_X = \sum F_Y = 0 \tag{4.34}$$

- The sum of forces on the Thialf, including the towline force, in the Thialf coordinate system must equal zero,

$$F_{x,Thialf} = F_{T,environmental,x} + F_{towline,x,Thialf} = 0, \tag{4.35}$$

$$F_{y,Thialf} = F_{T,environmental,y} + F_{towline,y,Thialf} = 0. \tag{4.36}$$

- The sum of forces on the Panamax, including the towline force, in the Panamax coordinate system must equal zero,

$$F_{x,Panamax} = F_{P,environmental,x} + F_{TurboSail,x} + F_{Propeller} + F_{rudder,x} + F_{towline,x,Panamax} = 0, \tag{4.37}$$

$$F_{y,Panamax} = F_{P,environmental,y} + F_{TurboSail,y} + F_{rudder,y} + F_{towline,y,Panamax} = 0. \tag{4.38}$$

(p) Output: Maximum Sailing Velocity
If the force balance for the moving coordinate system, Thialf and Panamax is confirmed, the maximum sailing velocity is reached and the program will create a file containing all system parameters, forces, moments and velocities and their development through the calculation steps.

5

Model Verification

The model is built up step-by-step to verify whether the reaction of all bodies in the model to every type of loading are as expected. After the completion of the model, it is taken apart to verify whether the separate parts still react as it should.

Three main functions of the model should at least be verified:

- Force and moment determination.
- Vessel movement verification
- Balance check.

Apart from the three main verification methods, two more measures to get an insight into the working of the model are implemented:

- Visualization of the movement up until balance.
- Force development throughout iteration steps.

In this Chapter the verficiation steps are carried out.

5.1. Force and Moment Determination

In the previous chapter it is explained how every force in the model is approximated and on which parameters the loads depend. The goal of the first verification step is to prove that every force is correctly calculated based on the parameters provided by the model in combination with vessel specific input data as presented in appendix B and C.

For this verification step, the Thialf is removed from the model and the Sailing Tug position and orientation are fixated within the moving reference frame. By this measure, the angles of attack for every environmental load on the vessel are equal to the chosen direction with respect to the moving reference frame. The velocity of the moving coordinate system is fixated as well. The direct relationship between model-input and calculated forces by the model can be checked manually.

First the above waterline forces determination is checked by exposing the Sailing Tug to wind only, resulting in a load on the hull above water and the Turbosails. Checks are performed for 3 predefined angles of attack and 2 incoming velocities. The values provided by the model proved to be identical to the manually calculated values. A numerical overview including the used coefficients for manual calculation is presented in table E.1 in appendix E

A second check for the Sailing Tug is implemented to verify the moments determined by the model around the vessel geometric centre. To check these moments the Panamax body is fixed to the reference frame by a moment sensor in the vessel geometric center. The sum of the moment generated by the current on the hull and the moment resulting from the forces provided by the rudder angle at the vessel aft, calculated by hand using formulas 4.15, 4.26, 4.27 and 4.28, should be equal to the value provided by the sensor. This appeared to be the case and the used numerical values and results can be found in can be found in table E.2 in appendix E.

Since the routines to calculate loads from waves, wind and current on both the Thialf and Sailing Tug are identical, the load determination in the model is assumed to be correct.

5.2. Vessel Movement Verification

With the verified force determining routines, the next step is to check the movement in the system resulting from these forces.To do so, a verification routine based on the Thialf is written. the Thialf body is connected to a towline-bridle combination as in the complete system. The point of the towline which is usually attached to the Panamax aft is now connected to a fixed point in the moving reference frame. When applying a single environmental load to the Thialf in start position ($\beta = 0$), the Thialf should gradually move to a position where no force perpendicular to the Thialf heading exist. Since the pivot points will be the point where the towline is connected to the reference frame combined with the symmetry of the Thialf underwater hull, it should obtain a position in line with the applied load.

Since the system velocity is set to zero for this test-case, the residual force in vessel specific x-direction, F_x, is directly related the coefficients from the input tables combined with the environmental velocity. The resulting values can be found in table E.3 Appendix E.

All presented values are confirmed by hand-calculation based on velocity combined with the coefficients from the input tables and are found to be correct, confirming that the model movement and current force calculation is correct. Since the forces and movement for both vessels in the model are determined using the same method, correct movement for both bodies is assumed.

5.3. Force Balance Check

The third verification is based on the complete model including the Sailing Tug and the Thialf. The goal is to prove that the combination of parameters found by the model:

- Sailing velocity
- Thialf drift angle
- Panamax drift angle
- Rudder angle

Provide a force balance for the complete system. For this verification multiple test cases are selected marked with red dots in polar plot 5.1. In the next chapter a graphical overview present in the system in X- and Y-direction is provided. Appendix E gives and overview of the numerical values and the sum in both X- and Y-direction. The sum of all forces in both direction proved to approach zero.

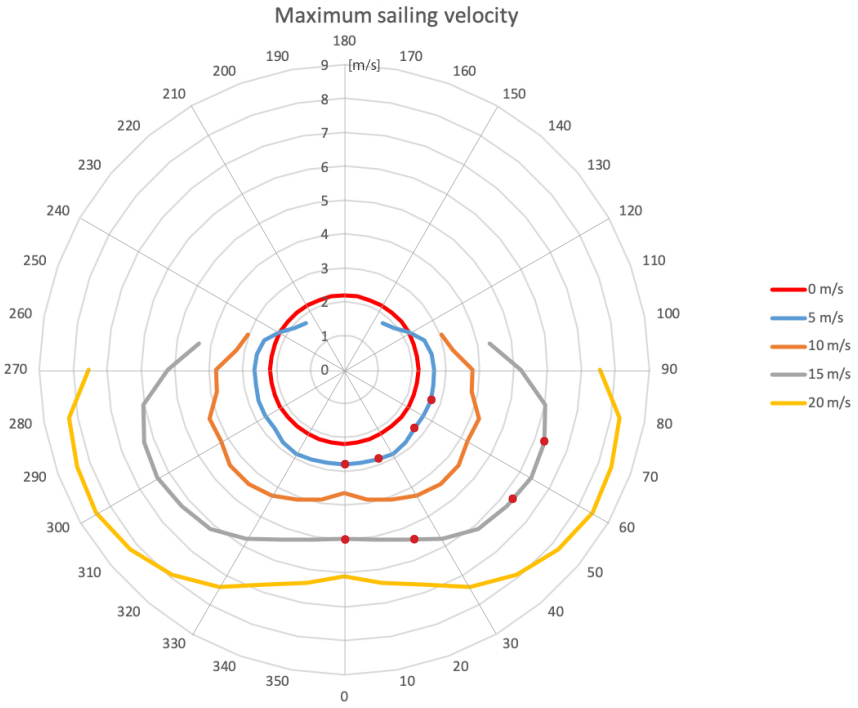

Figure 5.1: Maximum sailing velocity under different wind velocities

5.4. Visualization of Model Movement

The previous sections provided a verification of the force and moment determination in the model, the movement resulting form these forces and the final equilibrium position of the system. Additional measures are implemented to verify the behaviour of the system in the calculation steps in-between the start and equilibrium conditions. The first method to do this is the visualization of the moving coordinate system. From the start of the simulation, an overview of the moving coordinate system is displayed providing the opportunity to check whether the movement of both vessels is as expected. See figure 5.2

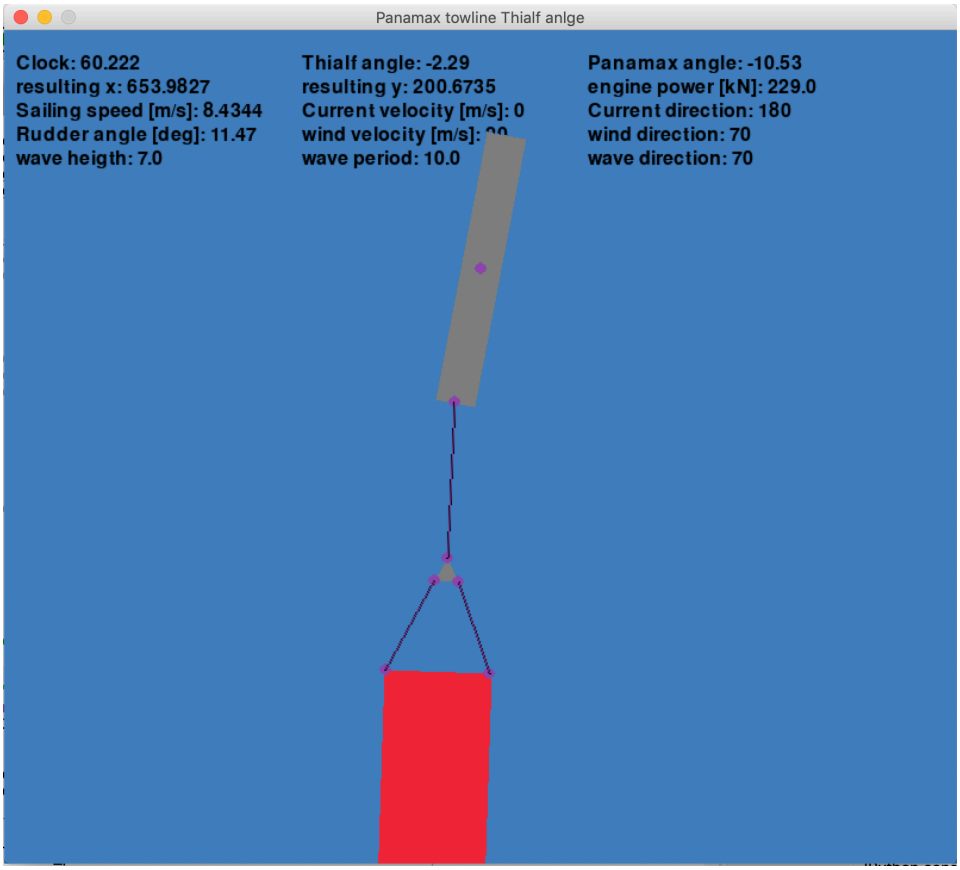

Figure 5.2: Moving coordinate system view

5.5. System Force Development

For every loop through the flow diagram, intermediate values for forces, moments, velocities and angles are recorded, providing the opportunity to check the calculated values by hand during every step and visualizing the development of every separate force in the system. Figure 5.3 to 5.8 show the force development for a wind velocity of 10 m/s with a 30 °wind direction relative to the sailing direction. Figure 5.3 shows the force components working in global X-direction on the Thialf, figure 5.4 in Y-direction. Figure 5.5 and 5.5 do the same for the Panamax. Finally figure 5.7 and figure 5.8 show the sum of forces for both vessels combined in global X and Y direction respectively. From these figures can be derived that the force development is logical and the sum of forces for X and Y converges to zero.

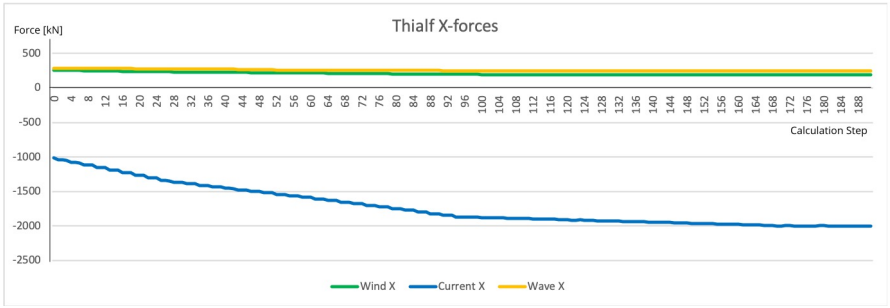

Figure 5.3: Thialf X force

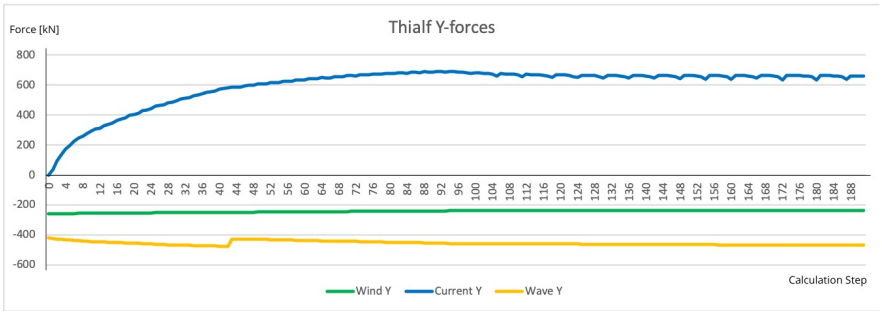

Figure 5.4: Thialf Y force

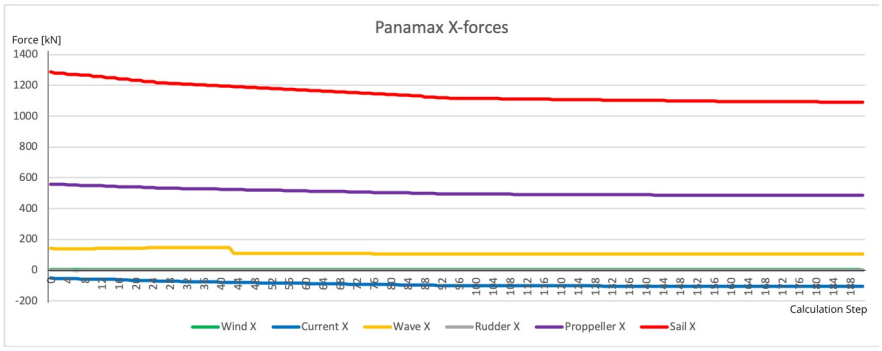

Figure 5.5: Panamax X force

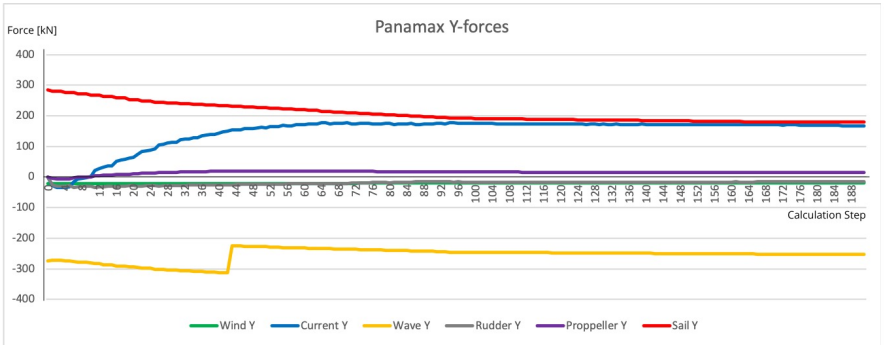

Figure 5.6: Panamax Y force

Figure 5.7: Resulting X force

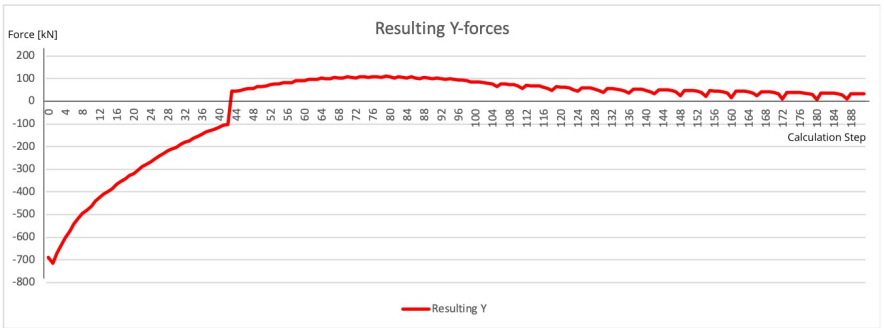

Figure 5.8: Resulting Y force

6

Results

The constructed VPP provides an enormous amount of output data, as a datapoint is created for every theoretical sailable combination of environmental conditions. While tabular output can be useful to look up specific values, this will not provide a practical overview of the system performance. A common method to present the output of a VPP is a polar diagram, as it provides an overview of the system performance at various windspeeds and angles in one figure. We chose to present the output of the VPP for the system performance through polar diagrams in Section 6.1 and 6.2.

Since we look at waves and wind as input, and sailing velocity, which directly relate to the water velocity around the hull, as output, an assumption about the relation between wind and waves must be made to be able to plot the output in polar diagrams. The relationship as provided by the International Marine Contractors Association (IMCA) will be assumed, which states that the wave direction will always be equal to the wind direction and links wave period and significant height to the prevailing wind velocity. As such, the wind velocities with the corresponding IMCA wave conditions are presented in Table 6.1.

Wind Velocity (m/s)	Significant wave height (m)	Wave period (s)
5	1.78	4.89
10	3.21	6.57
15	5.07	8.25
20	7.26	9.87

Table 6.1: Wind velocity and corresponding IMCA wave conditions

The system performance is assessed for wind velocities up to 20 m/s, which is found to be the wind-range experienced on common Thialf transit routes using SafeTrans, a voyage weather simulation software package. The wind velocity distribution can be found in figure 6.1 and an overview of the considered transit routes is displayed in Appendix H.

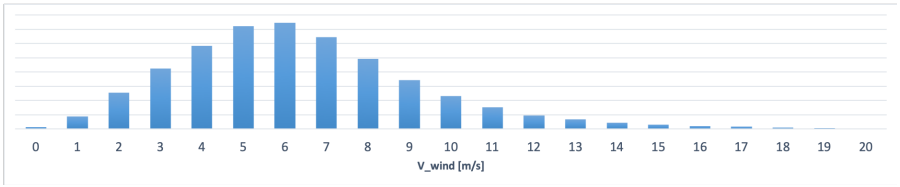

Figure 6.1: Wind distribution on common Thialf transit routes

6.1. Initial Results

The maximum sailing velocity of the system in 0, 5, 10 ,15 and 20 m/s wind are presented in Figure 6.2. The distance outwards (i.e. radially) from the centre of the plot represents the sailing velocity in m/s, the polar angle is defined as the wind direction relative to sailing direction. 0°wind direction means running with the wind, 90°or 270°will be beam reach.

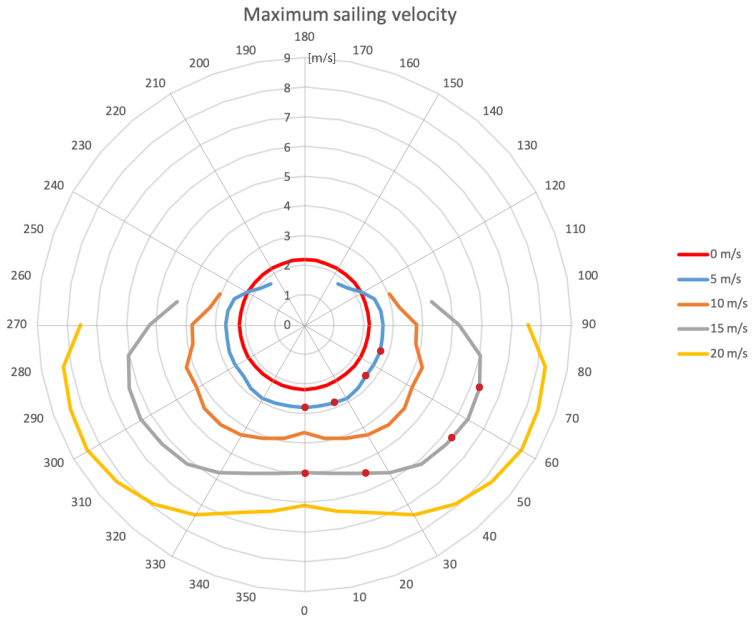

Figure 6.2: Maximum sailing velocity under different wind velocities

The sailing velocity under 0 m/s wind condition can be easily checked manually, since the are only forces present in the X-direction which consist of:

- Water-resistance on both underwater hulls,
- Air resistance on both hulls above water,
- A force on the 6 Turbosails,
- Propeller thrust under an inflow velocity equal to the sail velocity.

From the model output it is derived that $V_{max}(0m/s) = 2.19m/s$. When substituting this velocity and all 180°coefficients in the force calculation formulae, the sum of forces can be determined by hand. In table 6.2, an overview of these coefficients and the resulting forces is presented.

Coeff.	Value	Force	Value [kN]
$C_{T,c,x}$	-145.300	$F_{T,c,x}$	-695.780
$C_{P,c,x}$	-0.054	$F_{P,c,x}$	-33.130
$C_{T,w,x}$	-3.680	$F_{T,w,x}$	-17.620
$C_{P,w,x}$	-0.807	$F_{P,w,x}$	-0.370
$C_{Sail,x}$	-0.046	$F_{Sail,x}$	-0.840
J	0.004	F_{prop}	747.750
		Sum	0.000

Table 6.2: Coefficients and forces for a 0 m/s wind velocity force calculation

A striking observation from Figure 6.2 is the limited sailable angle relative to the wind. A possible explanation could be that the system is underpowered. As soon as the wind comes from an angle where it generates a negative force on the Thialf and Panamax hull, $90° < \alpha_{wind} < 270°$, the system is not able to obtain a positive velocity. We recall from section 2.1 that the combined installed power in a conventional tow setup is 45000 kW compared to 9470 kW for the proposed wind-assisted setup.

6.1.1. Separate Force Contributions

Given the system performance as presented in Figure 6.2, forces causing this performance are analyzed in further detail. Figure 6.3 to Figure 6.6 provide an overview of all forces present in the simulation for test-cases marked with a red dot in Figure 6.2. As a check the sum of all forces on both vessels is manually summed and proved to be zero in the X and Y-direction. Numerical values can be found in appendix E.

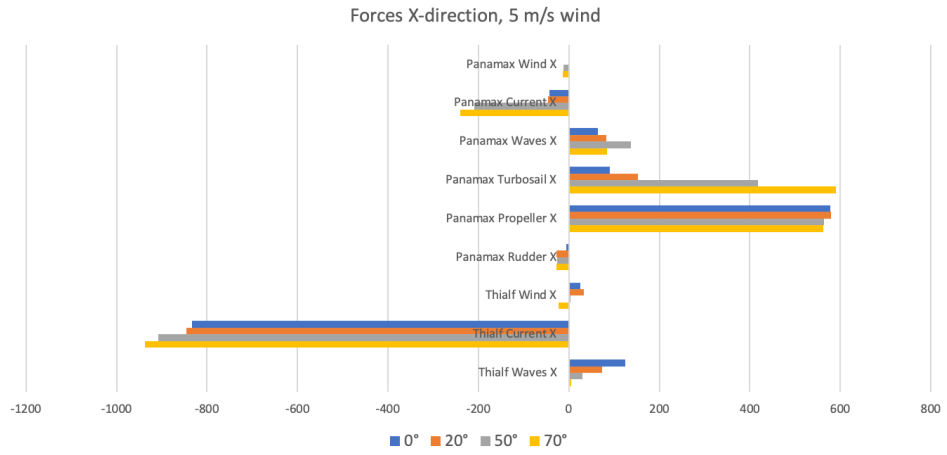

Figure 6.3: Forces X-direction 5m/s wind

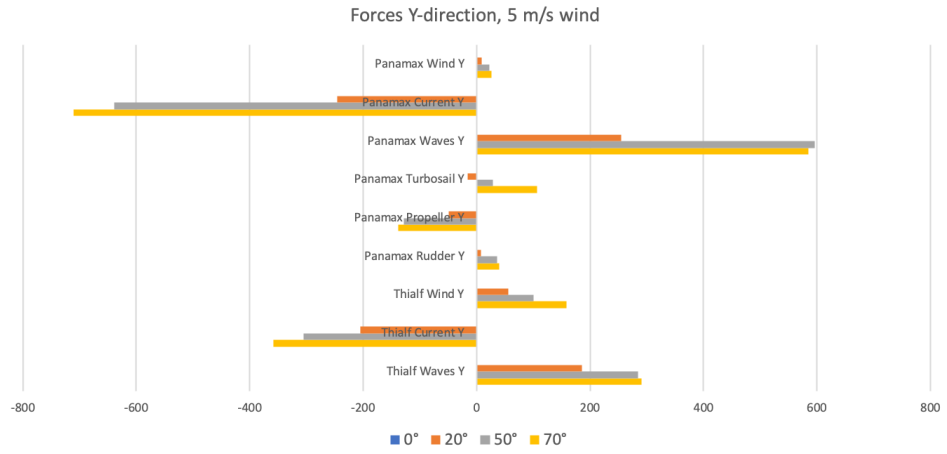

Figure 6.4: Forces Y-direction 5m/s wind

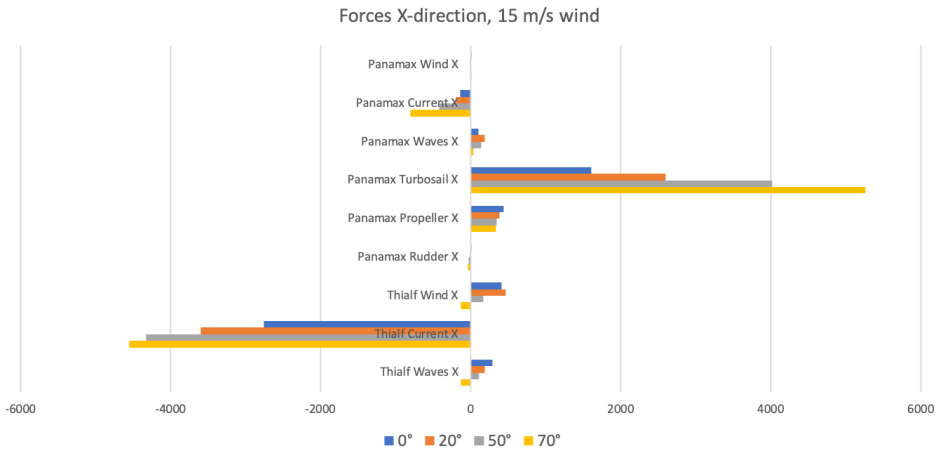

Figure 6.5: Forces X-direction 15m/s wind

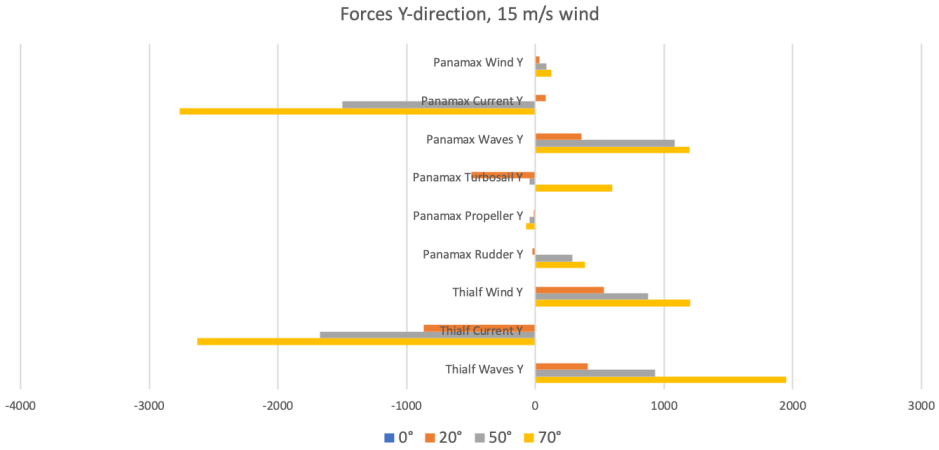

Figure 6.6: Forces Y-direction 15m/s wind

Figure 6.3 presents the forces present in the X-direction; the direction of movement. For the Thialf, only loads resulting from wind waves and current are present, where the Panamax has additional rudder, propeller and Turbosail contributions.

The dominant force for this 5 m/s case is the hull resistance from the Thialf, which is compensated by the positive force contributions of the propeller and the Turbosails. The Thialf resistance is relatively stable at the different wind angles, the small increase in resistance for larger wind angles can be explained by the increase in sailing velocity for wind angles towards beam reach, where the Turbosail lift force has a larger contribution, as well as the increase of the Thialf drift angle as the wind will push the Thialf sideways. The inverse relation can be observed for the propeller. An increase in sailing velocity will increase the inflow velocity which will decrease the propeller performance by the K_t relationship presented in Figure 3.4 in section 3.2.3.

The largest sensitivity to wind angle can be found in the Turbosail force contribution in the X-direction. For a 0°wind angle the Turbosails yield a force equal to only 90 kN, where for a 70°angle this force increases to nearly 600 kN, larger than the propeller contribution. This is a result of the fundamental properties of lift-creating devices like sails.

The challenge for every wind powered vessel usually is not associated with the force balance in sailing direction but more often lays in the balance perpendicular to the sailing direction.

Moreover, the goal is to be able to sail in every direction, but the presence of a perpendicular resulting force will prevent this.

Figure 6.4 gives an overview of the forces perpendicular to the direction of sailing, in the Y-direction under a 5 m/s wind. As both vessels are assumed to be symmetric, there will be no forces is this direction for a running wind condition (0°). For larger wind angles the wind and waves are expected to exert a positive load on both vessels, pushing the system leewards. These forces need to be compensated by negative forces induced by the drift angles β_P and β_T.

First of all, the sum of forces in the Y-direction for every wind angle is 0, confirming that there is a balance. The next notable attribute is the large wave contribution. From the Table 6.1 it can be deducted that 5 m/s wind results in a significant wave height of 1.78m with a wave period of 4.89 seconds with the direction of travel equal to the wind direction. From Appendix C, the maximum coefficient for wave force on the Panamax for an encounter frequency of 5 seconds is found to be 184.74 $(kN/m)^2$. This yields a force equal to 585 kN, indicating that the magnitude of the force is correctly obtained from the table. As expected, the Panamax hull is sensitive for beam wave drift forces. The drift-angle of the Panamax needed for sufficient leeward force has a side effect that the Panamax will turn to a position perpendicular wind and waves where it will experience beam waves.

Another unexpected result is the negative Y force delivered by the Turbosails at a 20 °wind angle as a result from the lift force created by the sails. Although unexpected, this has a positive result since the Turbosails partly counteract the negative Y-force on the Thialf and Panamax hull.

When the data of the X and Y force are combined into a leeward force to drag ratio, a value of 3 is obtained. To create a leeward force using a drift angle, the Panamax hull resistance in sailing direction increases by a third of the created leeward force.

Figure 6.5 and 6.6 give an insight in the X and Y forces within the system when sailing under 15 m/s wind conditions providing a 5.07m significant wave height and a 8.25 second period through the IMCA relationship.

The most noticeable difference in comparison with the 5 m/s force overview is the magnitude of all forces. Since both hydrodynamic and aerodynamic forces have a quadratic relationship to velocity, this is in line with expectations. For a wind angle of 20°, the sailing velocity of increases from 2.8 m/s for 5 m/s wind velocity to 5.3 m/s for 15 m/s wind velocity. As a result, the resistance of the Thialf increases from approximately 850 kN to 3000 kN.

The reason for the lower increase in sailing velocity compared to wind velocity arises from the fact that the sailing velocity depends on parameters other than global wind velocity. First of all, there is the change in apparent wind angle. An increase in sailing velocity will have a negative effect on the apparent wind experienced on the vessel as explained in section 4.3. Secondly, the propeller thrust has an inverse relationship to the sailing velocity as explained in section 3.2.3

Due to this lower increase in sailing velocity, the relative effectiveness of the Panamax and Thialf drift angle to create leeward force reduces for increasing wind velocities. To achieve a balance, an increase in drift angles is needed increasing the resistance even further and therefore reducing the sailing velocity.

6.1.2. Turbosail Thrust Contribution

Now it is clear what the maximum sailing velocity will be under different environmental conditions and which forces are the reason for these sailing velocities, a more detailed view on the Turbosail contribution in X-direction is provided by figure 6.7. When running downwind, the drag component is the main force provider for the Turbosails. The drag component is small compared to the maximum lift coefficient, one of the specifications on which the Turbosails were selected. Despite the low sail force contribution the system is still capable of maintaining a reasonable transit speed as seen in 6.2. This can be explained by the fact that especially the Thialf hull has a very large area exposed to the wind, such that the wind pushes the system forward.

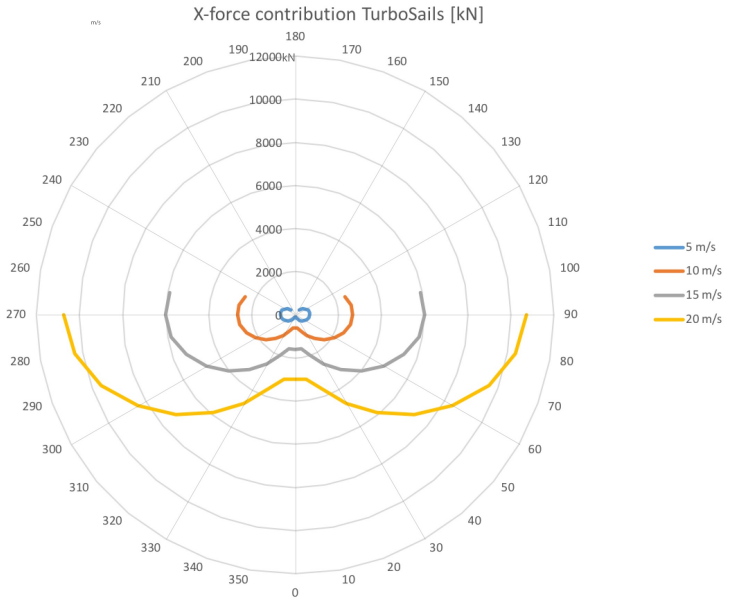

Figure 6.7: Force in X-direction from Turbosails

6.1.3. Panamax Drift Angle

The Panamax drift angle is the main measure to solve the balance in X-direction. The required yaw-moment to obtain a drift angle is provided by the rudder force component perpendicular to the vessel centerline combined with the rudder location with respect to the geometric center. While the drift angle does generate the compensating force to reach an equilibrium in the Y-direction, it does increase the hull resistance in the X-direction. Since a Panamax is not designed to efficiently deliver leeward force under a drift angle, large drift angles are required with a resulting large resistance in sailing direction. Figure 6.8 shows the Panamax drift angle for the sailing velocities plotted in figure 6.2.

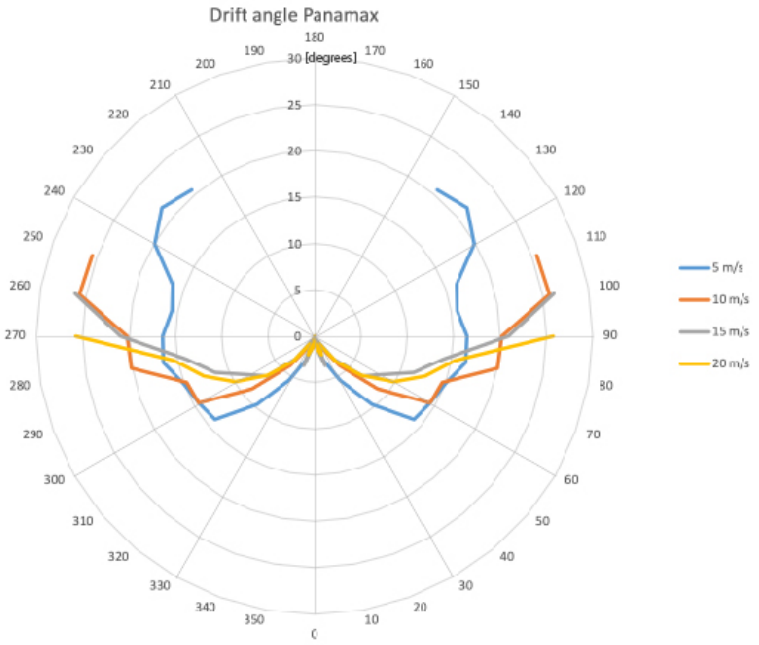

Figure 6.8: Associated Panamax drift angle under different wind velocities

6.1.4. Effective Rudder Angle

To create figure 6.9, a sign change is applied for rudder angles under wind angles $\alpha_w > 180°$ for visualization purposes, making it easier to check the system's symmetry. A first look at the rudder angle at different wind angles shows that the effective rudder angel α_R tends towards 25°for the ultimate direction with respect to the wind. For a wind condition of 5 m/s the rudder angle shows a graduate development for an increasing wind direction where for higher wind condition the increase in rudder angle tends to be steeper. A steep increase in rudder angle indicates that under those conditions the rudder angle might not be the an effective method to generate a sufficient yaw-moment. For broad reach wind conditions, $\alpha_W < 30°$ or $\alpha_W > 330°$, a negative rudder angle can be observed. These angles can be explained by the fact that the lift created by the sail partly pulls the system upwind as seen in figure D.2 in Appendix D.

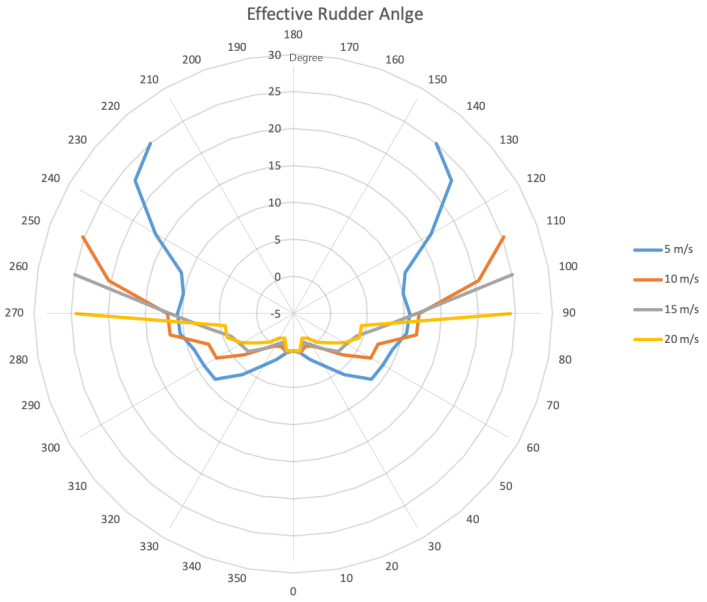

Figure 6.9: Effective rudder angle

6.1.5. Wave Influence

To test the influence of the waves resulting from the IMCA relationship, A calm water plot is created. Figure 6.10 shows the maximum sailing velocity when wave drift forces are not taken into account. An increased sail angle can be observed, especially for higher wind velocities. The explanation for this can be found in the implemented IMCA relationship between wave height and wind velocity.

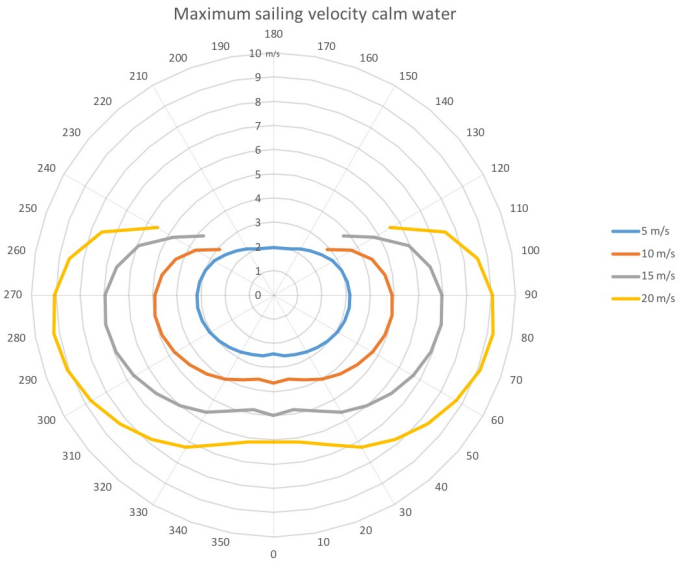

Figure 6.10: Maximum sailing velocity under different wind speeds without waves

6.1.6. Sailing Without Sails

To gain insight into the added value of the Turbosails, the performance is simulated for the Thialf-Panamax combination without Turbosail. Although the Turbosail do not provide a sailable system, they double the sailable angle of the system.

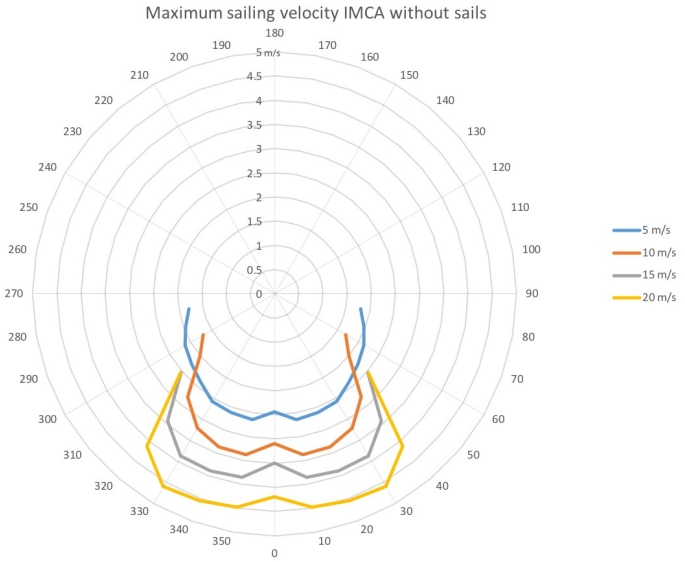

Figure 6.11: Maximum sailing velocity under different wind speeds without Turbosails

6.2. System Improvement Measures

The previously plotted results shows the system performance in the base case. These results also provide insight in possible points of improvement. With the previous conclusion that the first system configuration does not provide a feasible towing operation, the goal is to research possible improvements/refinements to the system. The main goal is to increase the sailable wind angles. Three improvements are proposed:

- Towline Attachment Adjustment
- Increase Engine Propulsion
- Application of a Trim Angle
- Removal of the Front Sail
- Mirroring of the Front Sail
- Thialf Thruster Propulsion

6.2.1. Towline Attachment Adjustment

Previous results showed the large effective rudder angles needed for the Panamax to adopt a sufficient drift angle. One of the explanations can be found in the drift-angle counteracting effect of the towline force. When the Panamax heading is not in line with the towline, an arm will arise, resulting in a moment on the Panamax. This towline moment needs to be compensated with the rudder, increasing the required rudder angle. Attaching the towline to the Panamax geometric center will remove the arm and therefore the moment on the vessel. The expected result is a reduced rudder drag and thus a higher sailing velocity, and a wider sailable wind angle since a larger drift angle can be adopted for the maximum effective rudder angle.

To check the effect of the towline, a simulation for an adjusted system with the towline

connected to the Panamax geometric center is executed. Theoretical this measure is easy to implement but this will be much more difficult in practice where the towline experience hindrance by the masts and other obstacles present on deck.

The towline connected in the geometric centre of the vessel yields the following simulation results presented in Figure 6.12.

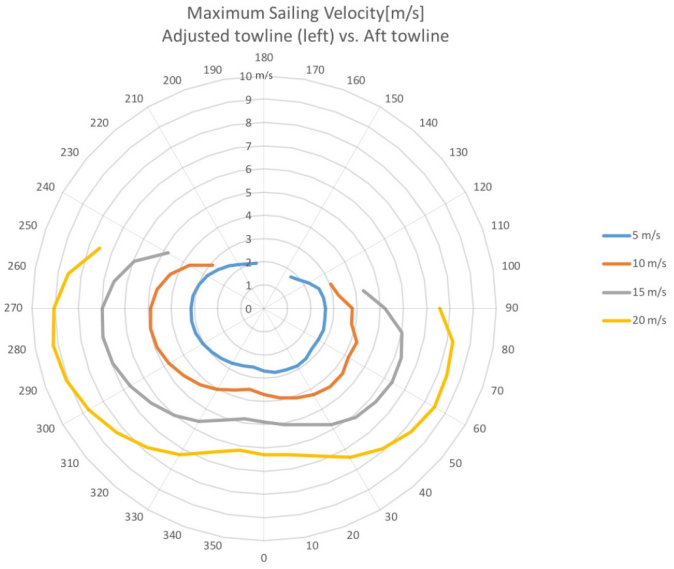

Figure 6.12: Maximum Sailing velocity with central towline attachment (left) vs. original towline setup (right)

6.2.2. Increased Engine Propulsion

Another observation of the first simulation results is that the leeward force balance is the main failure mechanism. Increasing the Panamax propeller propulsion can positively contribute to this balance in two ways. Firstly, the additional thrusts will increase the sailing velocity which in turn will increase the sideways generated force by the hull under a drift angle. This effect might be substantial due to the exponential relationship between inflow velocity and hull-generated force. Secondly the propeller thrust in line with the Panamax heading. While sailing under a drift angle there will be a component of the propeller thrust acting in the Y-direction.

To check the effect of an increase in propeller thrust, a simulation is performed where the delivered thrust of the Panamax is doubled. The result can be found on the left side of the polar plot below compared to the original configuration on the right side.

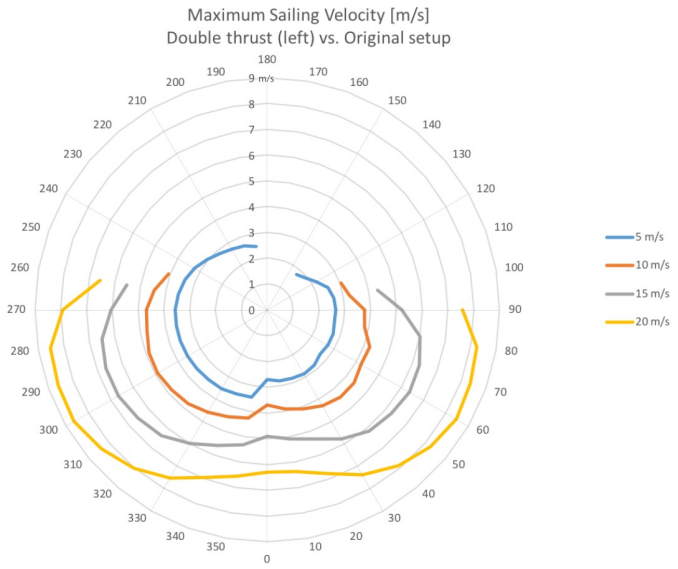

Figure 6.13: Sailing velocity with double installed thrust (left) vs. original towline setup (right)

6.2.3. Sail Layout Improvements

For the third area of possible improvement, the initial sail layout is reviewed. At the start of this research the sail area is maximized based on the Panamax stability. Upon simulating various combinations of input variables, the results revealed that the maximum sail thrust configuration did not provide an overall force balance. There are two mechanisms contributing to this failure.

- The force perpendicular to the sailing direction was larger than the hull generated Y-force under a drift angle.
- The needed yaw-moment to adopt a sufficient drift angle was larger than the yaw-moment the rudder was able to provide.

The Turbosail layout has a significant influence on both the leeward force in the system and the yaw-moment on the Panamax. For beam reach wind conditions, the conditions where the system fails, the sail drag force is working perpendicular to the sailing direction. Under this same condition, the location of the Turbosails with respect to the vessel geometric center provide to opportunity to manipulate the overall yaw-moment. The frontmost sail will be the most effective way to control the yaw moment due to the large arm with respect to the geometric center. Therefore, the sail lay-out improvements are applied on this specific sail.

Application of a Trim Angle

The first attempt to improve the sail performance using the sail layout is the implementation of sail trimming, a method to adjust the sail-generated forces. The sail induced forces can be influenced in two different ways. The first option is to change the ventilator power to manipulate the suction power. In section 2.3.2 is already mentioned that the generated forces can be reduced by approximately a factor 10 when the ventilation power is decreased and the sail-angles are trimmed.

Hcini et al. (2017) performed a numerical simulation of the Turbosail and compared the lift- and drag coefficients of a case with suction to a case without suction for various angles of incidence. For a 24 °angle of incidence, a negligible decrease in lift force is found and an increase in drag force coefficient of 138%. For a 48°angle of incidence, the lift coefficient decreases by 40% while the drag coefficient increases by 178%. Since the drag force only has a positive contribution to the propulsive force of the system when sailing windward and this is not the range where the system fails, it is concluded that decreasing aspiration power is not an effective measure to improve the systems performance.

The second option is to manipulate the wind angle of attack on the sails by varying individual sail angles. Earlier in this research the force resulting from the Turbosails is based on the F_X and F_Y Values provided by (Nelissen and Mao, 2016). With this data only it is impossible to implement the effect of individual sail-angle manipulation. To be able to implement individual sail trim manipulation, the effect the original lift and drag coefficient as found by (J.A. Cousteau, 1985) are used, Appendix D.

We still assume the values provided by Nelissen and Mao (2016) are the optimal setting for maximum forward thrust. The goal is to implement the change in resulting force when the sails are trimmed from this optimal thrust angle to decrease the leeward force from separate sails and thereby influence the yaw moment around the geometric centre of the vessel.

Another assumption is that for the optimal thrust setting, the Turbosails are oriented in such a way that the aerodynamic yield is maximal, so angle of incidence equals $20° < \alpha < 37°$. Which is most likely the case for the beam reach conditions where the initial system fails.

C_l and C_d values determined by Cousteau show an approximate linear relationship with the angle of incidence for the range $5° < \alpha < 37°$. Using this relationship, the trim-angle, which is a variation in angle of incidence can be converted to a lift and drag correction factor. To do this, the first step is to determine the average derivative for both the lift- and drag coefficient. This is done by a linear approximation of the coefficients provided by J.A. Cousteau (1985) for $5° < \alpha < 37°$ yielding the following results,

$$C_l = 3.0903 + 0.1502 * \alpha \tag{6.1}$$

$$C_d = 0.1634 + 0.0583 * \alpha \tag{6.2}$$

Taking the derivatives gives the correction factor for both coefficients,

$$\frac{dC_l}{d\alpha} = 0.1502 \tag{6.3}$$

$$\frac{dC_d}{d\alpha} = 0.0583 \tag{6.4}$$

Under the assumption that the original C_X and C_Y values will use the Turbosails in a way that they have a high aerodynamic performance, the correction is only valid for negative trim angles. Increasing the angle of attack will otherwise result in $\alpha > 37°$ where boundary layer separation occurs and the lift effect largely vanish.

With the lift and drag correction factors determined above, it is possible to calculate the lift and drag force penalties.

Since the original Turbosail force is provided in the global coordinate system, the lift and drag penalties must be converted to this coordinate system so they can be added to the original Turbosail force values.

1. Calculate trim force penalty based on trim angle ϵ

$$\Delta F_l = 0.1502 * 0.5 * \rho * A * \epsilon * V_a^2 \tag{6.5}$$

$$\Delta F_d = 0.05830 * 0.5 * \rho * A * \epsilon * V_a^2 \tag{6.6}$$

2. Convert lift and drag force to moving coordinate system using wind angle γ

$$\Delta F_X = -sin(\gamma) * \Delta F_l + cos(\gamma) * \Delta F_d \tag{6.7}$$

$$\Delta F_Y = -cos(\gamma) * \Delta F_l + sin(\gamma) * \Delta F_d \tag{6.8}$$

3. Add to original Turbosail force

$$F_{X,t} = F_X + \Delta F_X \tag{6.9}$$

$$F_{Y,t} = F_Y + \Delta F_Y \tag{6.10}$$

4. Convert to Panamax local coordinate system for force application (using rotation matrix):

$$F_{x,t} = cos(\beta_P) * F_{Y,t} - sin(\beta_P) * F_{X,t}) \tag{6.11}$$

$$F_{y,t} = sin(\beta_P) * F_{Y,t} + cos(\beta_P) * F_{X,t}) \tag{6.12}$$

Sail trim angles from 0 to -20°are applied to the original system failure cases to see which trim angle results in the maximum sailing velocity. The model determined this trim angle to be 0°for each case. Trimming the front sail angle will not have a positive effect on the system performance. An explanation can be found in the fact that the decrease in lift-force is three times bigger then the decrease in drag.

V_wind m/s	$\alpha_{w,max,original}$ deg	V_s m/s	ϵ_{maxV} deg	V_s m/s
5	140	2.93	0	2.93
10	110	3.54	0	3.54
15	100	4.25	0	4.25
20	90	6.61	0	6.61

Table 6.3: Front sail trim angle for maximum sailing velocity

Removal of the Front Sail

Since sail trim for the front most sail did not provide an improvement in sailing velocity, a more drastic approach to decrease the leeward force is implemented by completely removing the front sail from the vessel. This will decrease the total Turbosail, and thus the Turbosail leeward force by 17%.

Just as with the sail trim method, the point of engagement will shift towards the vessel aft, contributing to the yaw-moment needed for a drift angle.

Figure 6.14 shows a minor increase in sailing angle, but an overall decrease in sailing velocity due to the decrease in sail area.

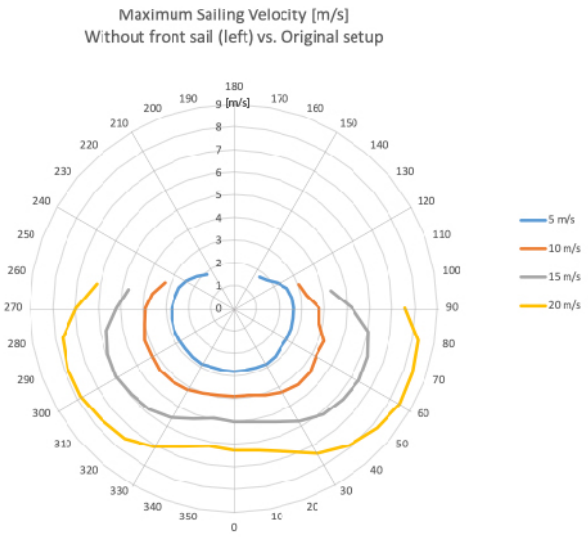

Figure 6.14: Sailing velocity without front sail (left) vs. original setup (right)

Mirroring the Front Sail

During discussion on the result, the idea arose to mirror individual sail orientations with respect to the incoming wind angle to create a lift force to the opposite direction. Using this method, the Sailing Tug moment and force balance can be manipulated. Again, this method is applied to the front most sail due to the maximum arm for which the mirrored lift force will create a moment on the Panamax in favorable direction for the drift angle.

To implement the option in the model, the first step is to calculate the lift-force from the global defined sail X- and Y-force using moving coordinate system wind direction γ

$$F_{lift} = -sin(\gamma) * F_{X,turbosail} + cos(\gamma) * F_{Y,turbosail} \tag{6.13}$$

The sail mirroring is implemented as a correction factor on the original sail force.

$$F_{lift,correction} = -2 * F_{lift} \tag{6.14}$$

The factor -2 is to remove the original lift force and replace it with a force in the opposite direction. The next step is to convert the lift correction factor back to the global coordinate system.

$$\Delta F_{X,mirror} = -sin(\gamma) * F_{lift} \tag{6.15}$$

$$\Delta F_{Y,mirror} = -cos(\gamma) * F_{lift} \tag{6.16}$$

The final step is to convert the global X and Y forces to the Sailing Tug coordinate system for application.

$$F_{x,mirror} = cos(\beta_P) * F_{Y,t} - sin(\beta_P) * F_{X,t} \tag{6.17}$$

$$F_{y,mirror} = sin(\beta_P) * F_{Y,t} - cos(\beta_P) * F_{X,t} \tag{6.18}$$

The results of the sail mirror method are tested for the wind-angles where the original layout failed can be found in the table below.

V_{wind} m/s	$\alpha_{max,original}$ deg	V_s m/s	$\alpha_{max,mirror}$ deg	V_s m/s
5	140	1.82	120	2.93
10	110	3.05	100	3.54
15	100	4.34	90	4.25
20	90	7.52	80	6.61

Table 6.4: Mirrored front sail sailing velocity

The sail mirror method did not improve the sailable wind angles for the system. The reason for this is that the system fails for wind angles close to beam reach conditions. For these wind angles the lift force is approximately in line with the movement direction. By mirroring a sail, the lift force becomes a negative force, slowing down the system, and the leeward drag force working on the Sailing Tug does not change.

When we look at the case for 15 m/s wind with a global angle of attack of 100°, the total Turbosail propulsive force will decrease from 5918 kN to 4561 kN. The resulting relative yaw-moment around vessel geometric center from the mirroring of the front sail is -31437 kNm. The propulsion penalty is large when compared to the rudder drag penalty for this case. The 24°rudder angle for this case provides a -76431 kNm moment around the vessel geometric center with a drag penalty of 397 kN.

6.2.4. Sailing with Thialf Propulsion

Based the previous results can be concluded that a tow-configuration without using the propulsion is unfeasible. To propose a functional tow configuration, a setup is tested including propulsion from the 6 thrusters available on the Thialf.

The direction of the delivered thrust is assumed to be in line with the Thialf heading, to approximate the best case scenario, the amount of thrust is based on the thrusters MCR.

The Thialf thruster K_t values are available inhouse at HMC and are used to determine the thrust based on the inflow velocity. The relationship between thrust and inflow velocity is linearized using the same method as for the Panamax, explained in section 3.2.3. The Thialf thruster K_t values and the linearization can be found in Appendix B.13.

Comparing the radial distance in figure 6.15 provides insight in the velocity gains from the Thialf propulsion. The system benefits most in wind directions other than broad reach conditions and for smaller wind velocities.

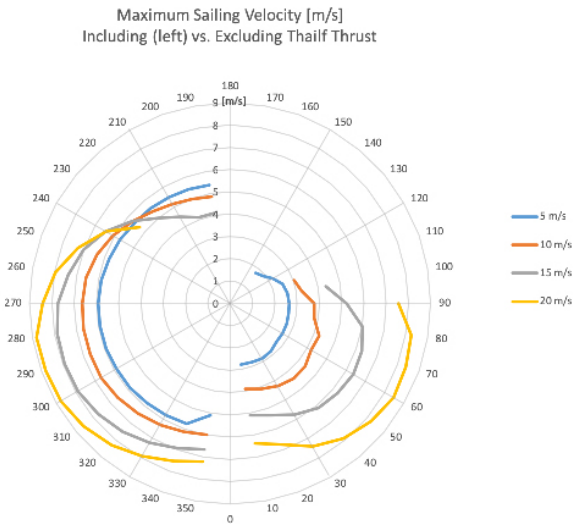

Figure 6.15: Sailing velocity without front sail (left) vs. original setup (right)

7

Conclusion

The goal of this research was to investigate the possibility to apply wind-assisted towing to the Thialf transit operation in order to reduce the carbon footprint. For this purpose, a design of a wind-assisted tow vessel named the Sailing Tug was proposed which was based on a discarded Panamax hull. The behavior of the Sailing Tug in configuration with the Thialf was simulated to answer the following research question,

Is it feasible to replace the Tug present in a conventional tow configuration by a wind-assisted Tow Vessel and tow the Thialf without using its own installed thrusters?

The design requirements for a feasible tow configuration were determined to be a positive sailing velocity for relative wind angles $\alpha < 135°$ and $\alpha > 225°$, as described in section 1.2.

Simulation results for the initially designed configuration indicated that this system does not meet the design requirements. Thus, in answering the research question, this research indicates that is not feasible to replace the conventional tow configuration by a wind-assisted tow vessel to tow the Thialf without using its own installed thrusters. A separate force analysis during the simulation indicated that the failure of the initial system is due to the imbalance of forces perpendicular to the movement direction of the system. Replacing a conventional tug by the wind-assisted tug design introduces a large leeward force on the sails and the Panamax hull. Furthermore, the larger dimensions of the Panamax vessel compared to a conventional tug in combination with the IMCA assumption that the incoming wave direction is equal to the wind direction further increases the leeward force on the towing vessel under beam reach wind conditions, the conditions where the system was found to start failing.

The main measure to compensate for this leeward force is to adopt a drift angle for the Panamax tow vessel, but initial results showed that the compensating force generated by the underwater Panamax hull was limited compared to the force generated by wind, waves and the towline exerted on the Panamax.

The relation between the sailing velocity and the generated force presented the main failure mechanism for the wind-assisted tow configuration, as illustrated in Figure 7.1.

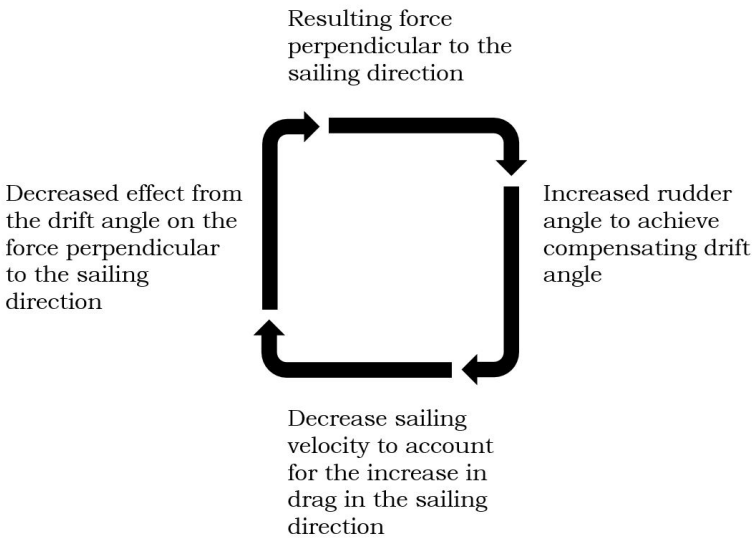

Figure 7.1: wind-assisted Towing failure scenario

Based on the conclusion that the initially designed system does not meet the design requirements, multiple measures of improvement were implemented and tested to determine their effect on the system performance.

7.1. Course-Keeping at Lower Sailing Velocities

The relationship between sailing velocity and leeward force indicated by the results of the simulation also provides insight in the system's behavior for sailing velocities lower than the maximum velocity under specific environmental conditions. Where the Panamax hull-generated leeward force has an exponential relationship with the incoming water velocity, and thus sharply decreases for lower sailing velocities, the leeward force caused by wind and waves does not decrease to the same extent. When the required propulsion is lower for tow operations, the sails can be trimmed such that the drag decreases, but the leeward force on the Panamax hull caused by wind and waves remains largely the same. Thus an imbalance of forces perpendicular to the movement direction exists at low system velocities. Separate force analysis showed that the Turbosail generated leeward force is relatively small compared to the wind and wave forces exerted on both the Thialf and Panamax hulls. As a result, the designed configuration is unsuitable for propulsion in a tow operation, where lower transit velocities are desirable at some intervals.

7.2. Towline Contribution to Panamax Yaw-moment

The simulation indicated that a second problem in the designed wind-assisted tow configuration is caused by the towline yaw-moment exerted on the Panamax. It was found that the point of attachment of the towline on the Panamax stern results in an increasing arm of the towline-force when the difference between the towline angle and the Panamax drift angle increases. By this mechanism the Panamax is pulled in line with the towline, an effect that can be compensated to some extent through the rudder, but that will induce a rudder drag penalty. The counteracting moment from the towline is unfavorable since it requires a drift angle for the Panamax to create a sufficiently large leeward force in the system.

7.3. Transverse Hull Force

The main obstacle in wind-assisted towing is the required compensation of the force perpendicular to the sailing direction. Due to its dimensions, the results indicated that the Panamax does not have a suitable underwater body to efficiently create a compensatory force. The large Panamax drift angles required to produce the leeward force result in a large increase in hydrodynamic drag. The leeward force generation efficiency of the Panamax hull can for example be improved through the application of fins on the keel, or through the design of a dedicated hull with a longer and more v-shaped underwater body. Investigation of such improvements to the Panamax design are recommended for further research.

7.4. Sum-Up

- The initial system lay-out of the Sailing Tug-Thialf combination does not meet the defined design requirements for a feasible tow operation.
- The system requires a high minimum sailing velocity to keep course, which is undesirable in a tow operation.
- The overall force and moment presence in the system makes is hard to achieve a balance. Especially the towline force exerted on the Panamax stern requires compensation through a large rudder angle, inducing a large rudder drag.
- Due to the Panamax hull dimensions it is inefficient in leeward force generation, such that investigation in the application of fins or a dedicated wind-assisted tow vessel hull design are recommended to improve the leeward force generation.

7.5. Effect of System Improvement Measures

Based on the results on the performance of the initial wind-assisted configuration a number of improvement measures were proposed in consultation with HMC with the aim to design a system that meets the design requirements.

7.5.1. Towline Attachment Adjustment

To avoid the negative towline yaw-moment contribution on the Panamax, the towline attachment point was moved to the vessel's geometric centre. Theoretically this is an easy adjustment but practically this introduces difficulties due to the living quarters and the Turbosails present on deck. The measure did improve the sailing performance. The maximum sailable direction relative to the wind roughly improves by 20%, but the configuration still does not meet the design requirements.

7.5.2. Increased Engine Propulsion

It was found that doubling the Panamax engine propulsion to increase the engine performance widened the sailable wind direction due to the larger sailing velocity, and thus the larger hull generated side force. Another positive effect was observed in the propeller thrust contribution in the Y-direction under a Panamax drift angle. When a proportional relationship between fuel consumption and delivered thrust is assumed, the fuel consumption approaches the value of the conventional setup, leaving little improvement in carbon footprint. A higher Panamax thrust increases the towline-tension and therefore has larger counteracting effect on the Panamax drift angle. The positive effect of the increased Panamax propulsion was most noticeable under small wind velocities, the effect decreased for increasing wind velocities due to the exponential relationship of the wind induced forces.

7.5.3. Sail Lay-out

The third investigated area for improvement was the sail layout. At the wind directions where the initial system failed, broad reach wind conditions, the location of the Turbosails on deck can have a large influence on the yaw-moment. The front sail is the is the sail with the largest drift-angle counteracting moment due to its position in front of the vessel geometric center and large arm. Therefore sail layout variation were tested for this sail. Three scenarios were implemented:

1. Application of a Trim Angle,
2. Removal of the Front Sail,
3. Mirroring the Front Sail.

Application of a Trim Angle

The sail trim method is implemented as an adjustment of the Turbosail orientation, turning it away from the maximum aerodynamic yield angle. This will decrease both the lift and drag produced by the sail. Results showed that the sail trim angles up to 20°did not significantly improved the sailing performance. A reason for this, is the fact that the change in produced lift force is approximately three times larger than the change in drag. For beam reach condition, the lift force has a positive effect on the system performance where the drag provides an unwanted leeward force. The favorable yaw-moment induced by the front sail trim angle was limited compared to the rudder induced yaw-moment.

Removal of the Front Sail

With the conclusion that the sail trim method did not bring the required improvement in sailing performance, a more drastic variation in sail layout was implemented by completely removing the front sail. This measure decreased the total sail area and moved the wind-force point of engagement even further to the ships aft, which contributes to the yaw-moment needed for the Panamax drift angle. This setup demonstrates a small increase in sailable directions and a minor decrease in overall sailing velocity, as presented in figure 6.14. The expectation was that a decrease in sail area, and the associated reduction of leeward force of 17%, combined with the shift in point of engagement with respect to the vessel geometric center would have a significant impact on the system performance. This proved to be not the case. On one side the leeward force of the Turbosails is only one of the factors in the leeward force balance, the wave- and wind-forces on the Panamax hull play an even more dominant role in the Y-balance. Secondly the method of sacrificing one Turbosail to create a relative yaw-moment has a propulsion penalty larger than the rudder drag penalty to create the same moment. By these results the assumption is raised that the rudder is a more efficient method to control the yaw-moment on the Panamax. An additional measure to increase the system performance could be to increase the rudder area and with that the rudder generated yaw-moment.

Mirroring the Front Sail

The implementation of the sail mirroring method proved to have no positive effect on the system performance. The sailable wind angle decreases and the sailing velocity for beam reach conditions is lower then in the original setup.

7.5.4. Sailing with Thialf Propulsion

The considered system improvement measures did not bring the required performance improvement, therefore is was decided to step away from the original research question and asses the feasibility of a wind-assisted tow configuration including the Thialf installed propulsion. The Thialf thrusters are used at their MCR, significantly increasing the propulsion force present in the system. This measure contributes to an improved system performance in multiple ways.

- The additional thrust will increase the sailing velocity
- The increased sailing velocity will increase the hull generated leeward force under a drift angle
- The tension in the towline will be smaller
- Both the lower towline tension and higher sailing velocity will increase the effectiveness of the rudder to manipulate the Panamax yaw-moment and therefore drift angle

Using the Thialf installed propulsion is the most effective considered method to increase the system performance. From the polar can be concluded that the system will be able to meet the criteria declared in chapter 1.2 for wind velocities up to 20 m/s. Although the fuel saving opportunities will largely vanish by this method.

7.6. Discussion

This research shows that the use of a wind-assisted tow configuration based on a Panamax, without using the Thialf propulsion is not feasible. The model developed to check the configuration performance provides a comprehensive method to test variations in the tow-configurations for different environmental conditions.

A method to improve the sailing performance is to switch on the Thialf propulsion, although this contradict the original research motivation, reducing the carbon footprint of Thialf transit operations.

The main point of failure is the required force balance transverse to the sailing direction. The Panamax basis used for the preliminary wind-assisted tug design proved to be not the optimal base case due to the limited leeward force generation under a drift angle.

The concept of using a discarded Panamax vessel as a basis for a sailing tug seemed a promising option for various reasons. First of all, the combined application as floating breakwater and sailing tug has a cost advantage. Research by P. Smulders (2017) proved the feasibility for the use of a Panamax as floating breakwater. While the concept proved to be feasible, it would financially unattractive to sail a separate vessel to a project location only for this use. Using the Panamax as a Sailing Tug during transit could provide a solution for this problem. Another opportunity is the low transit velocity during transit, contributing to favorable apparent wind angles. The great stability of a Panamax vessel enables the option to apply a large sail area.

Simulations showed that the Panamax hull will not be the ideal basis for a sailing tug. Where the large dimensions create a large stability and therefore enables the application of a large sail area, an associated drawback is the large sensitivity to environmental loading. The difficulties to come to a leeward force balance does not only arise from the leeward force created by the Turbosails, wave and wind forces on the Panamax hull showed to be an even more dominant factor.

The second problem with the Panamax hull is the low course stability. Most sailing vessels have a strong v-shaped hull with a deep keel or fins, increasing the leeward force generation when sailing under a drift angle. The flat bottom of the Panamax bulk carrier proved to be inefficient in creating leeward force.

It is up for debate whether a wind-assisted tow configuration is a feasible option at all. The large required roll-stability to compensate the heeling moment from the installed sails will require large vessel dimensions. These large vessel dimensions will unpreventably increase the sensitivity to environmental loading. The sensitivity to external conditions and the corresponding lack of ability to control forces vectors in the configuration is undesirable in a tow-operation from an operational perspective. The procedure to attach the towline to both vessels for example requires precise movement and position holding capabilities, this is hard to do with a wind-assisted vessel. Another negative characteristic is the unpredictable transit duration, especially with an expensive vessel like the Thialf.

Bibliography

Dykstra Naval Architects. The ecoliner concept. *Status Report July*, 2013.

Lloyd Bergeson and C Kent Greenwald. Sail assist developments 1979–1985. *Journal of wind engineering and industrial aerodynamics*, 19(1-3):45–114, 1985.

Volker Bertram and Herbert Schneekluth. *Ship design for efficiency and economy*. Elsevier, 1998.

Curtze C.A. Brockett, W.A. Bureau of ships journal. *vol 12, no. 1*, 1964.

KMJ Drenthe, GR Dekker, LJ Kemp, and DAM van Velzen. Propellers performance in oblique flow. *Delft University of Technology*, 2016.

P. S. Dykstra. Using a breakwater in offshore operations. *Graduation thesis TU Delft*, 2017.

Hitoshi Fujii. Experimental researches on rudder performance. *Journal of Zosen Kiokai*, 1960 (107):105–111, 1960.

Anne Harris. the shape of ships to come. *Engineering & Technology*, 8(6):44–45, 2013.

Cherif Hcini, Essia Abidi, Badreddine Kamoun, and David Afungchui. A turbosail profile analysis code based on the panel method. *Energy*, 118:147–155, 2017.

F.C. Bosveld en A. Stepek H.W. van den Brink, I.L. Wijnant. Klimatologie van extreme windvlagen. *WR 2017-01*, 2017. URL `http://bibliotheek.knmi.nl/knmipubWR/WR2017-01.pdf`.

J. Constans J.A. Cousteau, B. Charrier. Foundation cousteau and windship propulsion. *Journal of Wind Engineering and Industrial Aerodynamics*, 20:39–60, 1985. doi: 0304-3908/85.

JMJ Journée, WW Massie, and RHM Huijsmans. *Offshore Hydromechanics: Course OE4630*. TU Delft, 2000.

Pinkster J. Journee, J.M.J. Introduction in ship hydromechanics. *Delft University of Technology*, 2002.

Omer Kemal Kinaci, Abdi Kukner, and Sakir Bal. On propeller performance of dtc post-panamax container ship. *International Journal of Ocean System Engineering*, 3(2):77–89, 2013.

Jukka Kuuskoski. Norsepower rotor sail solution. 2017.

Jialun Liu, Frans Quadvlieg, and RG Hekkenberg. Impacts of rudder profiles on ship manoeuvrability. 2015.

Köhler Nelissen, Traut and Mao. *Study on the analysis of market potentials and market barriers for wind propulsion technologies for ships*. CE Delft, 2016.

G. Nijsten and J. Vos. Propulsion aspects of large sailing yachts. *Proceedings of the 17th International Symposium on Yacht Design and Yacht Construction*, 2002, 2002.

OCIMF. Prediction of wind and current loads on vlccs, 1994.

P. S. Smulders. Using a breakwater in offshore operations. *Graduation thesis TU Delft*, 2017.

Michael Traut, Paul Gilbert, Conor Walsh, Alice Bows, Antonio Filippone, Peter Stansby, and Ruth Wood. Propulsive power contribution of a kite and a flettner rotor on selected shipping routes. *Applied Energy*, 113:362–372, 2014.

N. Troll. Application and feasibility of towing kites on hmc vessels. *Graduation thesis TU Delft*, 2010.

Erik A.J. Vroegrijk. Cfd current drag - ocimf. *Lloyd's Register*, page i, 2017.

Katarzyna Żelazny. An approximate method for calculation of mean statistical value of ship service speed on a given shipping line, useful in preliminary design stage. *Polish Maritime Research*, 22(1):28–35, 2015.

A

Sails

Square Rig

The square rig arrangement is used from simple single sails to the complex and sophisticated multiple sail rigs developed over 2,000 years ago for the major ships of war, commerce, and exploration. The primary driving sails are carried on horizontal spars which are perpendicular, or square, to the keel of the vessel and to the masts as illustrated in Figure A.1. From Figure A.2 it can be deduced that a maximum lift coefficient of 1.6 can be reached when sailing half wind (Bergeson and Greenwald, 1985). The main disadvantage of the square rig is the large crew needed to control this type of rig.

Figure A.1: Square rig ship

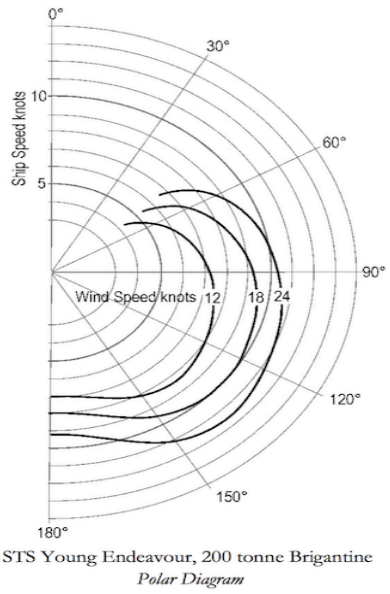

STS Young Endeavour, 200 tonne Brigantine
Polar Diagram

Figure A.2: Square rig polar diagram

Bermuda rig

Bermuda rigs are classic rigging as found om the majority of sailing yachts. From the 17th century onward, the Bermuda rig found its way to propel pure sailing vessels, dinghies/cruisers etc. The Bermudan rig is not the most aerodynamic sail-plan since it tends to have a very poor lift distribution as a result of the construction of the mast. The mast is supported by wires fore and aft that form two triangles, thus its sails must also be triangular in shape. Triangles are not a desirable shape for a lift-generating plane because of induced drag, which

comes as a product of any surface generating lift. The maximum lift capacity is 1.8 as stated by Bergeson and Greenwald (1985).

Dyna Rig

The Dyna rig sail design originates from work done by W. Proll in 1960 (Harris, 2013), and is based on the square rig. The main advantages of the Dyna rig setup are a high performance, the little maintenance required, high safety and the ease of use. The rig can be controlled by a single person from the bridge by rotating the masts. No additional crew members are needed (Dykstra, 2017). The most recent demonstration of this type of rig on a larger ship was the Maltese Falcon, as illustrated in Figure A.4.

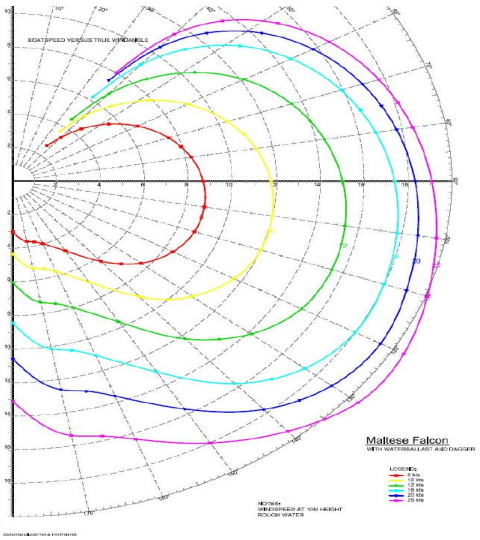

Figure A.3: Maltese falcon polar diagram

Figure A.4: Maltese Falcon

Aero rig

The Aero rig is the soft sail with the highest performance when compared to a three-mast schooner, Dyna rig and sloop setup with identical sail surfaces (Nijsten and Vos, 2002). The Aero rig improves the sail surface perpendicular to the wind. The challenge of this type of rig is the construction of the rotation point a the lower side of the single mast as this is the only fixation point to the vessel.

Kite

The drawback for kite propulsion is the limited sailing angle compared to other wind conversion systems.

Previous research on the subject of towing kites for HMC vessels (Troll, 2010) lead to the conclusion: “Based on best estimates it can be concluded that the towing kite system is not feasible on the HMC semisubmersibles at the current fuel prices. This is a consequence of the relative low thrust contribution of the towing kite, the large investment costs and the large replacement costs and low durability of the kite.”

Since the Oil price has significantly decreased since 2010 we assume that a towing kite is still no feasible solution for the application on SSCV’s.

C

Environmental Loading Coefficients Panamax

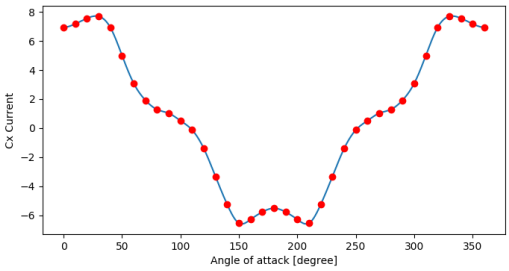

Figure C.1: Panamax current force x

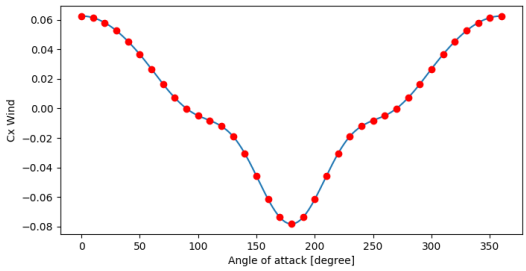

Figure C.2: Panamax wind force x

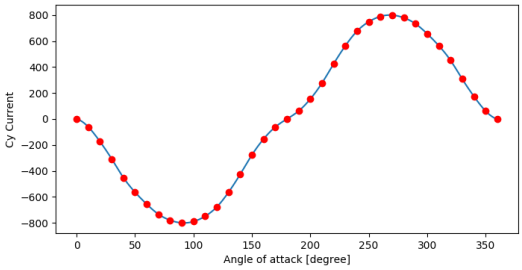

Figure C.3: Panamax current force y

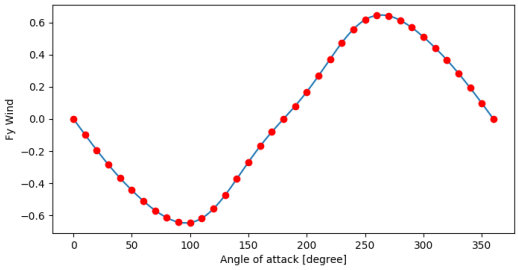

Figure C.4: Panamax wind force y

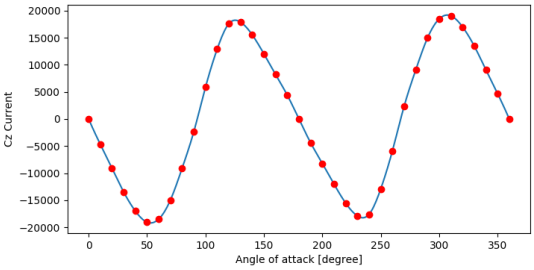

Figure C.5: Panamax current moment z

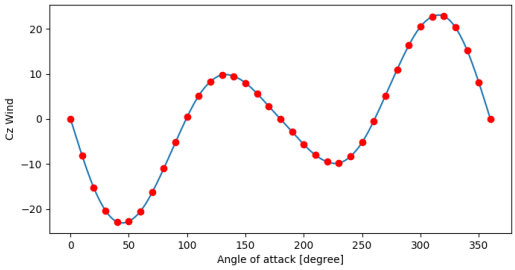

Figure C.6: Panamax wind moment z

Speed	Speed	Advance ratio	K_t	Thrust	Thrust estimated
knots	m/s	J		kN	kN
0	0	0	0.4468	750	750
1.916307	0.985833	0.1	0.3721	624.6083	690
3.832613	1.971667	0.2	0.3754	630.1477	630
5.74892	2.9575	0.3	0.3494	586.504	570
7.665227	3.943333	0.4	0.3215	539.671	510
9.581533	4.929167	0.5	0.2894	485.7878	450
11.49784	5.915	0.6	0.2572	431.7368	390
13.41415	6.900833	0.7	0.2235	375.1679	330
15.33045	7.886667	0.8	0.1898	318.5989	270
17.24676	8.8725	0.9	0.1501	251.9584	210
19.16307	9.858333	1	0.0817	137.1419	150

Table C.1: Panamax Thrust values at various Speeds

D

Turbosail Coefficients

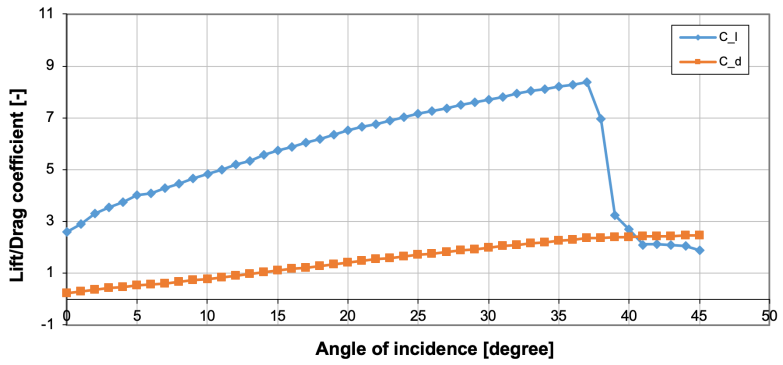

Figure D.1: Turbosail lift and drag coefficients as determined by J. Cousteau (J.A. Cousteau, 1985)

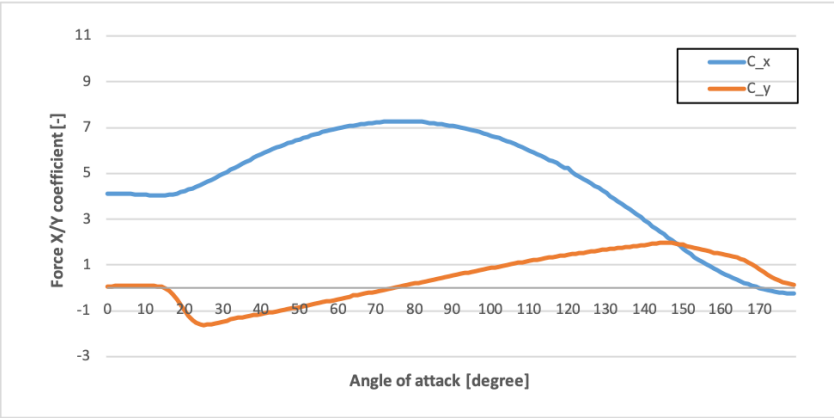

Figure D.2: Turbosail force coefficients for X and Y direction determined by (Nelissen and Mao, 2016)

E

System Verification

Wind		Model determined loads					Manually calculated loads					Coefficients							
alpha	V	Hull			Turbosails		Hull			Turbosails		Panamax						TurboSail	
		X	Y	Z	X	Y	X	Y	Z	X	Y	C_x	C_y	C_z	A_T	A_L	L_bp	C_X	C_Y
0	10	6255	0	0	270761	0	6255	0	0	270761	0	0.645	0	0	150	1000	229	3.589808818	0
50	10	3656	44350	-2265142	416876	65239	3656	44350	-2265142	416876	65239	0.377	0.686	-0.153	150	1000	229	5.52703335	0.864950731
270	10	-10	-64262	518170	456399	-40373	-10	-64262	518170	456399	-40373	-0.001	-0.994	0.035	150	1000	229	6.051027722	-0.535278388
0	30	56294	0	0	2436852	0	56294	0	0	2436852	0	0.645	0	0	150	1000	229	3.589808818	0
50	30	32904	399149	-20386278	3751888	587150	32904	399149	-20386278	3751888	587150	0.377	0.686	-0.153	150	1000	229	5.52703335	0.864950731
270	30	-87	-578359	4663528	4107589	-363360	-87	-578359	4663528	4107589	-363360	-0.001	-0.994	0.035	150	1000	229	6.051027722	-0.535278388

Table E.1: Panamax wind force verification

V_c	α_c	δ	α_R	$C_{z,T}$	M_{hull}	C_n	$F_{Y,rudder}$	M_{rudder}	$\sum M$	M_{python}
m/s	degree	degree	degree		kNm/(m/s)^2		kN	kNm		kNm
1	105	-50	25	33106.22	33106.22	-0.52	-30.81	-3374.20	29732.02	29732.02
2	120	0	60	39915.95	159663.78	-1.20	-294.17	-32212.15	127451.63	127451.63
3	150	15	45	23715.46	213439.10	3.34	-1403.70	-153704.91	59734.19	59734.19
4	195	-30	-45	-10866.73	-173867.66	-3.34	-506.69	-55482.91	-229350.57	-229350.57
5	255	60	-15	-33106.22	-827655.52	-2.55	3735.82	409072.83	-418582.70	-418582.70

Table E.2: Panamax hull and rudder moment generation calculated by hand vs. determined in Python model

Thialf

Wind		Current		Waves							
Direction	V	Direction	V	Direction	H_s	T	Thialf angle	F_x	F_y	M_z	M_towline
Deg	m/s	Deg	m/s	Deg	m	s		kN	kN	kNm	kNm
0	10	-	-	-	-	-	0	0	314.09	0	0
50	10	-	-	-	-	-	130	-0.01	-355.72	-0.06	-0.06
180	10	-	-	-	-	-	0	0.01	-355.73	0.07	0.067
270	10	-	-	-	-	-	90	-0.63	-355.73	-4.08	4.08
0	30	-	-	-	-	-	0	0	2826.82	0	0
50	30	-	-	-	-	-	130	-0.11682	-3201.55	-0.75	0.75
180	30	-	-	-	-	-		1.273366	-3201.55	8.20	-8.20
270	30	-	-	-	-	-		-0.04945	-3201.55	-0.32	0.32
-	-	0	4	-	-	-	0	0	2324.95	0.00	0.00
-	-	50	4	-	-	-	130	0.39	-1701	-11.94	11.94
-	-	180	4	-	-	-	0	1.59	-1701	-48.43	48.43
-	-	270	4	-	-	-	90	-1.01051	-1701	30.87	-30.87
-	-	0	6	-	-	-	0	0	5231.13	0	0
-	-	50	6	-	-	-	130	0.54361	-3827.26	-16.61	16.61
-	-	180	6	-	-	-	0	0.393783	-3827.26	-12.03	12.03
-	-	270	6	-	-	-	90	1.791694	-3827.26	-54.74	54.74
-	-	-	-	0	5	7	0	0	693.50	0	0
-	-	-	-	50	5	7	130	0.058033	-691	-1.93	1.93
-	-	-	-	180	5	7		0.042312	-691	-1.41	1.41
-	-	-	-	270	5	7		-0.04059	-691	1.35	-1.35
-	-	-	-	0	10	15		0	-999	0	0
-	-	-	-	50	10	15		-0.06172	-1011	-1.16	1.16
-	-	-	-	180	10	15		5.89E-06	-1011	0.00	-0.00
-	-	-	-	270	10	15		-0.06283	-1011	-1.18	-1.18

Table E.3: Thialf movement and force verification

V_{wind}	5	5	5	5	15	15	15	15
alpha	0°	20°	50°	70°	0°	20°	50°	70°
Thialf Wav X	123.86	74.06	30.31	4.80	295.74	186.65	113.17	-131.21
Thialf Cur X	-834.00	-844.95	-907.87	-937.89	-2754.35	-3596.99	-4330.06	-4551.87
Thialf Wind X	24.66	33.47	3.26	-22.27	417.18	464.45	167.72	-126.79
Pan Rudder X	-5.55	-26.83	-25.59	-26.98	6.87	-12.02	-29.43	-39.46
Pan Prop X	577.81	579.03	564.36	562.62	442.15	381.29	345.76	341.88
Pan Sail X	90.26	153.08	417.94	590.81	1613.82	2600.10	4021.33	5264.10
Pan Waves X	63.45	81.93	136.60	84.00	104.91	187.43	137.50	41.31
Pan Current X	-42.43	-45.65	-208.66	-240.07	-140.09	-196.31	-414.76	-807.08
Pan Wind X	-0.15	1.39	-11.40	-12.98	13.34	-8.00	-3.13	11.22
SUM	-2.09	5.54	-1.04	2.04	-0.42	6.59	8.11	2.12

Table E.4: X-forces balance verification

V_{wind}	5	5	5	5	15	15	15	15
alpha	0°	20°	50°	70°	0°	20°	50°	70°
Thialf Wav Y	0.00	185.59	284.59	291.04	0.00	405.47	928.56	1951.65
Thialf Cur Y	0.00	-205.34	-304.46	-358.48	0.00	-867.27	-1674.01	-2625.75
Thialf Wind Y	0.00	55.78	100.32	158.07	0.00	533.11	875.84	1204.98
Panamax Rud Y	0.00	8.27	36.59	39.98	0.00	-24.11	286.80	386.11
Panamax Prop Y	0.00	-49.76	-128.03	-138.10	0.00	-10.50	-42.66	-71.71
Panamax Sail Y	0.00	-15.57	28.74	106.75	0.00	-497.64	-42.73	599.13
Panamax Wav Y	0.00	254.51	595.57	584.70	0.00	359.92	1083.78	1199.66
Panamax Cur Y	0.00	-246.20	-638.58	-711.02	0.00	77.66	-1498.58	-2765.97
Panamax Wind Y	0.00	9.52	22.40	25.98	0.00	30.61	87.66	124.24
SUM	0.00	-3.20	-2.85	-1.08	0.00	7.25	4.66	2.34

Table E.5: Y-forces balance verification

H

Thialf Voyages

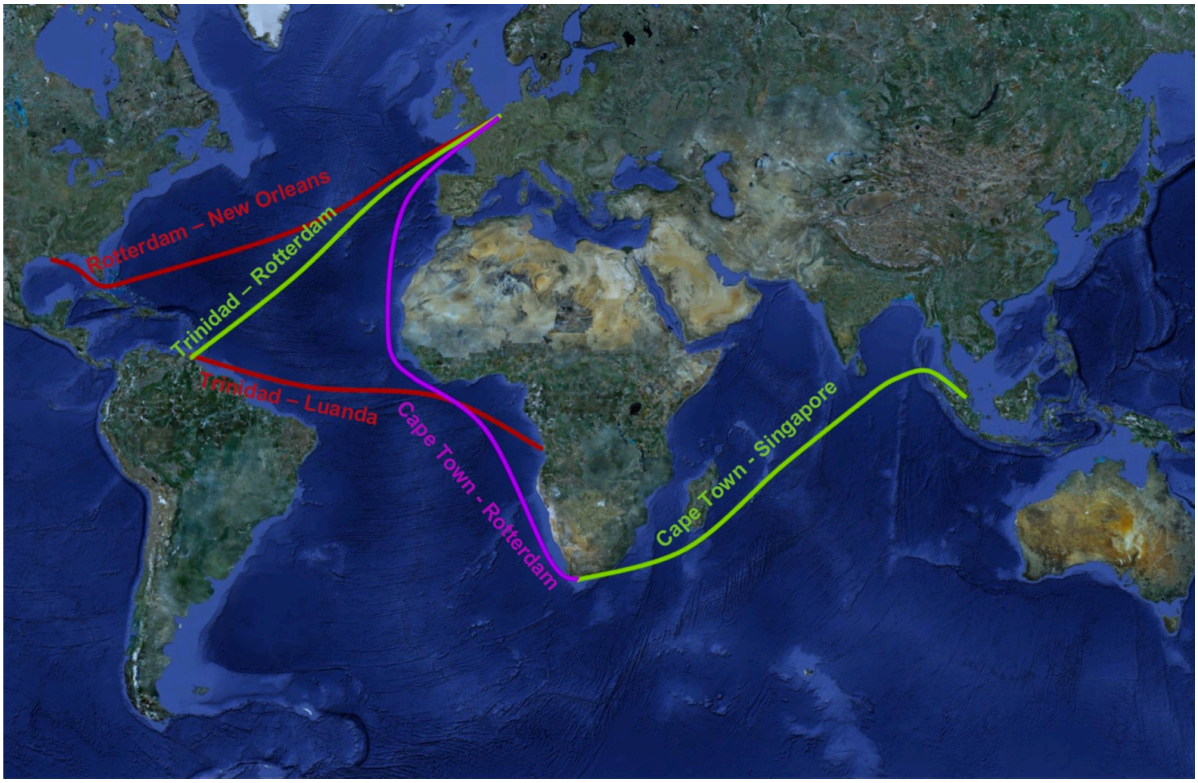

Figure H.1: Thialf common voyages